END
DATE
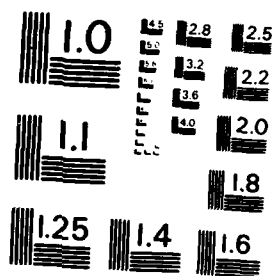FILMED
1 83
DTIC

MICROCOPY RESOLUTION TEST CHART
NATIONAL BUREAU OF STANDARDS - 1963 - A

ERL-0230-TM

AR-002-824

DEPARTMENT OF DEFENCE

DEFENCE SCIENCE AND TECHNOLOGY ORGANISATION

ELECTRONICS RESEARCH LABORATORY

DEFENCE RESEARCH CENTRE SALISBURY
SOUTH AUSTRALIA

TECHNICAL MEMORANDUM
ERL-0230-TM

ATMOSPHERIC WATER VAPOUR DIFFERENTIAL ABSORPTION
MEASUREMENTS WITH AN INFRARED SOUNDER

P.W. BAKER

DTIC
ELECTE
NOV 5 1982

A

Approved for Public Release

COPY No. 5

MARCH 1982

82 11 05 068

DEPARTMENT OF DEFENCE

AR-002-824

DEFENCE SCIENCE AND TECHNOLOGY ORGANISATION

ELECTRONICS RESEARCH LABORATORY

TECHNICAL MEMORANDUM

ERL-0230-TM

ATMOSPHERIC WATER VAPOUR DIFFERENTIAL ABSORPTION

MEASUREMENTS WITH AN INFRA-RED SOUNDER

P.W. Baker

S U M M A R Y

The atmospheric differential absorption by water vapour
between two CO_2 laser transmission lines has been measured
up to heights of 1.5 km with a groundbased sounder system.
Water vapour profiles, some containing distinct layers,
have been estimated from long and short pulse soundings,
and compared with radiosonde measurements. Strongly
scattering aerosol layers, often associated with
temperature inversions, cause severe distortion of the
long pulse differential absorption profiles, indicating
the necessity of using a short pulse technique. This
technique shows potential usefulness for the remote
measurement of radio refractive index layers in the
atmosphere.

TABLE OF CONTENTS

Page

LIST OF APPENDICES

1. INTRODUCTION

Task DST 77/116 has as its main aim the development of a Carbon dioxide (CO_2) infra-red laser sounder to measure water vapour profiles in the atmosphere. This report provides results of measurements up to November 1981 and documents the status of the program at that time. The conclusions presented will be of a tentative nature, pending further measurements and the publication of a subsequent report.

2. BACKGROUND

Following the advent of the laser, efforts were soon made to realise its potential for remote sensing of atmospheric constituents. Initial work was mainly on measurements of the concentration and structure of atmospheric aerosols by the LIDAR technique (Light Detection and Ranging). Later this technique was extended to utilise the principle of Raman spectroscopy in which each molecular species reradiates at a frequency which is uniquely offset from the exciting laser frequency. However, because of the low level of the reradiated Raman energy, this technique is not feasible in a daylight background.

Another technique, which utilises the frequency dependent absorption properties of water vapour on backscatter returns from atmospheric aerosols to determine water vapour content along the path, was developed by Schotland in 1964(ref.1). Although initially the method appeared to be limited by difficulty in achieving the necessary stability of the ruby laser transmission, these difficulties have now been overcome and other high stability lasers which are suitable for implementing the technique, such as the CO_2 laser, have been developed.

3. DIFFERENTIAL ABSORPTION AT LASER WAVELENGTHS

A wavelength tunable CO_2 laser is capable of tuning over many tens of discrete lasing frequencies which correspond to energy transitions in the CO_2 molecule.

Over the CO_2 band of emissions (9.4 to 10.8 μ) there is a continuous background absorption due to water vapour. However, there are also some discrete absorption lines due to water vapour which overlap some of the CO_2 lines and hence these CO_2 lines are more strongly absorbed by water vapour. The R(20) CO_2 line (10.2466 μ) is located in a water vapour absorption line and is much more strongly absorbed than any other CO_2 transmission line. This line has been used in conjunction with several other lines having lower absorption to measure the differential absorption along the transmission path.

The backscattered power detected by a lidar system can be expressed as(ref.1).

$$P_r = P_T\left(c\,\frac{\tau}{2}\right)\frac{A}{R^2}\,\beta(R)\,\exp\left(-2\int_0^R (\gamma + \rho K)\,dR\right) \qquad (1)$$

when

P_T = transmitted power per pulse (W)

c = velocity of light(m/s)

τ = pulse length (s)

A = receiving telescope aperture(m^2)

R = distance to scattering volume(m^2)

$\beta(R)$ = volume backscattering cross section (m^{-1} str^{-1})

$\gamma(R)$ = extinction coefficient (m^{-1})

K = absorption coefficient (m^{-1} atm^{-1})

$\rho(R)$ = partial pressure of absorbing species (atm) = $\dfrac{W}{0.622}$
where W is the mixing ratio(gms/gm).

An expression for the average concentration of the absorbing molecular species over the range interval ΔR is given by(ref.3)

$$\rho(R) = \frac{1}{2\Delta K \Delta R}\left(\ln\left\{\frac{P_1(R)}{P_1(R+\Delta R)} \times \frac{P_2(R+\Delta R)}{P_2(R)}\right\} + I + S\right) \qquad (2)$$

P_1 = unabsorbed power at wavelength 1

P_2 = unabsorbed power at wavelength 2

ΔK = difference between absorption coefficients of molecular species at two wavelengths

I = interferring material error

S = scintillation error due to wavelength variability of scatter.

In deriving equation (2) it has been assumed that the differences in the extinction and backscattering coefficients at the two wavelengths are negligible. This is a reasonable approximation for the CO_2 line pairs employed. A careful selection of the two wavelengths used for the absorption measurements will minimise the error, I, due to absorption by other molecular species. Errors due to scintillation are usually negligible over small wavelength ranges.

Since Schotland's initial experiment, the technique has been extended to the near infra-red (0.715 to 0.740 µ) with a ruby pumped dye laser and to CO_2 wavelengths (10.6 µ) where suitable water vapour absorption characteristics are available. Table 1 is a representative list of remote sampling measurements of atmospheric gases.

4. SOUNDER DEVELOPMENT

4.1 Equipment description

A block diagram of the sounder components is sketched in figure 1 The Lumonics TEA-103-2 laser together with the 30 cm Newtonian telescope is supported on a mobile steel carriage. Specifications for the sounder are given in Table 2.

The Laboratory in which the laser is housed has a one-metre square ventilation chute protruding through the roof. A cover is attached to this which can be slid off to one side on rollers to open the one-metre square aperture. The telescope points vertically through the centre of the opening.

The CO_2 laser is optically aligned approximately with the aid of a helium neon laser, which is inserted as indicated in figure 1. More precise alignment is subsequently carried out over a horizontal range with the aid of a target van. The procedure is described in Appendix I.

4.2 Radio frequency interference

Following laser and telescope alignment, and a demonstration that the laser performance measured with a target van was within the specified performance limits, a high sensitivity mercury-cadmium-telluride (CMT) detector, designed for operation at 77°K, was substituted for the P1-61 pyroelectric detector. Severe radio frequency (rf) pickup problems were then encountered, due to the relatively large body of the detector dewar and the high-gain, wide-bandwidth preamplifier (5 Hz to 10 MHz) which was attached to the dewar.

It was ascertained that the rf pickup from the 35 kV discharge of the laser power supply drove the preamplifier into saturation. This was of concern for two reasons. Firstly, there was subsequent distortion to any detected infra-red signal and secondly, there was was a danger of damage to the front end of the preamplifier, due to excessive signal levels. To reduce the rf radiation from the laser, a box shield was constructed around it, as shown in figure 2. This effectively meant the laser was double shielded, as its primary enclosure was specified as providing rf shielding by the makers. Although this procedure reduced the rf pickup on the detector by approximately 20 dB, there was still an undesirable level of rf breakthrough present. To reduce this further, a shield was constructed around the detector. Both the laser and detector were earthed at one point only to minimise earth current effects. The enclosure for the detector is shown in figure 3 (the telescope is to the right of the detector shield shown). Copper braid was inserted between contacts on all aluminium surfaces to reduce radiation leakage. The window in the side of the detector housing is to allow adjustment of the detector which is mounted on a carriage with adjustments available along 3 axes.

4.3 Wavelength calibration of laser

A spectrum analyser designed for use at CO_2 wavelengths (Optical Engineering CO_2 Spectrum Analyser) was employed for the calibration. As

- 4 -

the normal display scale is not able to withstand high power, it was
replaced by a carbon strip on which the beam impinged adjacent to the
wavelength scale markings. The scale calibration was initially checked by
using a helium neon laser as described in the handbook. The scale read
high by 0.007 microns and this was allowed for in the calibration. A
special platform was constructed to mount the spectrum analyser and a
90 degree light tube was built to direct the laser beam into the aperture
of the spectrum analyser. A carbon strip with a small aperture was placed
in front of the spectrum analyser to protect areas adjacent to the aperture
slit from the CO_2 beam.

The positions of several CO_2 wavelength lines on the CO_2 laser grating
micrometer scale were noted. It was later found that maintenance work on
the output optical system of the laser, or severe vibration of the
micrometer, alters the micrometer calibration, so that it is advisable to
recalibrate in these cases.

4.4 Digital recording of range intensity display

Brief details of all components of the laser sounding and digital recording
system are given in Appendix II. One of the initial recording problems
encountered was to sample the lidar return, which has a dynamic range of
approximately 40 dB, at rates greater than 5 MHz. Because of the
unavailability of high speed A/D converters with greater than 6 bit
sampling range at the commencement of the programme, it was decided to
perform a logarithmic amplification on the signal. As the detector output
voltage is directly proportional to the incident optical power, the
dynamic range of the detected signal (in dB) is twice that of the optical
power (in dB). Hence an A/D system capable of measuring a 40 dB variation
in optical power must be able to operate over a dynamic range of 80 dB.
With a 6 bit A/D, an electrical power resolution of 1.25 dB is obtainable,
corresponding to an optical power resolution of 0.625 dB. The logarithmic
amplifier response deviates from a logarithmic function at the bottom and
top of the ranges of operation. A calibration is shown in figure 4,
indicating a true logarithmic response over a 52 dB range.

The A/D device was also employed to monitor the transmitted laser pulse,
and is described in Appendix II.

4.5 Initial horizontal transmission tests with CMT detector

Following completion of shielding on both laser and detector, the system
was tested on the target van after inserting 40 dB optical attenuation in
front of the detector. Strong echos were received from the van showing the
relatively great improvement in performance obtainable from the CMT
detector compared to the pyroelectric detector.

The echo strengths received from the side of the van were measured for
three adjacent CO_2 lines, R(22) (10.233 µ), R(20) (10.247 µ) and
R(18) (10.260 µ). The measured water vapour absorption coefficients for
R(18) and R(22) are both low, and significantly less than for R(20)(ref.5).
The water vapour content of the atmosphere near the earth's surface was
calculated from wet and dry bulb temperature observations taken near the
transmission position. The predicted and measured differential absorptions
relative to R(20) were then compared. (The predicted differential
absorptions for R(18) to R(20) and R(22) to R(20) were very nearly equal).
In general the measured differential absorption for R(18) to R(20) was
slightly lower than predicted. This may have been due to slight changes in
laser beam transmission direction as the wavelength was changed by tilting
the diffraction grating. Measurements of the beam imprint on heat
sensitive paper at 10 m confirmed this as a likely explanation. Another

possible, but not likely, explanation is an additional differential
absorption effect due to another gas such as ammonia.

As the differential absorption was only of the order of 2 dB for the above
measurements (at 450 m range), the measurements were repeated at longer
ranges using the hills face as a target (shown in figure 5). Oscilloscope
photographs of echos are shown in figure 6, the range scale is 750 m per
division. However, in this case at a range of 3.5 km the absorption was
such that an R(20) echo could not be detected above noise level for single
pulse operation. This is to be expected, as the differential absorption,
in decibels, is directly proportional to range for a constant water vapour
content along the range, and therefore the absorption should be nearly
8 times the value for 450 m range, ie a value of 15 to 16 dB would be
expected.

It was concluded that the differential absorption effect on the sounder
performance was measurable over useful ranges.

5. VERTICAL MEASUREMENTS OF DIFFERENTIAL ABSORPTION

5.1 Introduction

During the horizontal transmission tests it was noted that strong
interfering echos were received from the structure supporting the roof
mirror. This was due to reflections, by this structure, of the forward
scattered laser beam. These reflections were reduced by covering as much
as possible of the structure with a non-reflecting material. However,
discernible echos still remained. Finally to reduce echos to a minimum a
75 mm diameter light pipe was used to completely enclose the laser beam,
until it cleared the roof hatch as shown in figure 7. However, when the
roof mirror was employed for horizontal transmissions, echos still
remained, probably due to reflections from the roof hatch, after the beam
had been reflected by the laser roof mirror. It was concluded that to
completely eliminate these echos for future horizontal sounding
measurements the laser beam would need to be completely enclosed until it
cleared the building. This step has not been taken to date because it is
intended that the system be mainly operated in the vertical mode.

5.2 Preliminary measurements

These consisted of digitally recording sequences of five-ten pulses of each
of the three CO_2 lines R(18), R(20) and R(22). The laser was operated with
a gas mixture of He and CO_2 only, which gives the shortest pulse length,
but at a lower power output than when nitrogen (N_2) is included in the mix.
Initial pulse echos from the target van, with different N_2 mixes, indicated
a considerable variation in the pulse length. Further direct measurements
on the emitted pulse showed a pulse length variation of over 10 to 1, with
the shortest pulses corresponding to the zero N_2 mix. The pulse length is
defined as the time taken to decay to a value of e^{-1} of its peak value.
The peak value of the pulse is reached within 50 ns for all gas mixes, but
the pulse decay varies between 100 ns for a zero N_2 gas mix, up to 1 µs for
a standard N_2 mix.

5.3 Effects of pulse energy and duration

Preliminary measurements indicated a range capability with the short pulse
of 800 m to 1 km before the differential absorption rate began to
apparently decrease with range. This condition is reached when the
differential absorption equals the signal-to-noise of the signal suffering
the least absorption, ie typically the R(18) transmission. When the long

pulse high energy mode was employed, this range limitation was extended out to beyond 1.5 km. However in this case, measurements at ranges less than 500 m indicated that range gated samples were often distorted by the contribution of backscattered energy in the tail of the pulse at the shorter ranges. Pulse tail effects are considered in Appendix III. The severity of this interference depends on the backscattering aerosol density profile. It is minimised when there is a low aerosol density decay with height, ie a large scale height.

5.4 Pulse averaging considerations

Initial measurements indicated there could be a considerable difference between successive sets of averaged differential absorption data, where each set was obtained from typically five pairs of pulses. Normal random variations were expected due to the random variations in aerosol distribution, but these differences indicated statistically non-stationary processes were occurring. It was therefore decided to add the capability of switching back and forth automatically between the selected pair of differentially absorbed wavelengths, so that non-stationary effects would be minimised. In the original concept of the microprocessor program, the intention was that the pulse triggering and line selection would be under program control. However, due to lack of staff resources, this facility has not yet been implemented. At present, periodic triggering sequences are generated by the laser control unit, running at a pulse repetition period of 13 s. The drive for the optical grating is also initiated by this trigger.

The width of a sampled range cell was 25 m, which was therefore the maximum resolution of the system. However, in processing the backscattered absorption data, it was found to be advantageous to compute a running average of the results over at least ten 25 m range cells to smooth out quantizing effects. Four different processing methods were used. In the first estimation method, the 25 m range cell water vapour estimates in grams/kilogram were smoothed over $2n + 1$ range cells obtained from the averaged power P for N pulse pairs in adjacent range cells, as follows:

$$W_j{}^{(1)} = \sum_{i=j-n}^{i=j+n} w_i = \frac{622}{2\Delta K \Delta R} \Sigma \log_e\left(\frac{P_{18}(r_i)}{P_{20}(r_i)}\middle|\frac{P_{18}(r_{i+1})}{P_{20}(r_{i+1})}\right) \tag{3}$$

where ΔK is a constant determined by the difference in the absorption coefficients for each line ($km^{-1}\ atm^{-1}$) and ΔR is the range interval (25 m).

The second processing method consisted of summing the power ratios over $2n+1$ cells before taking the logarithm, ie:

$$W_j{}^{(2)} = \frac{622}{2\Delta K \Delta R} \log_e\left(\sum_{j-n}^{j+n}\frac{P_{18}(r_i)}{P_{20}(r_i)}\middle|\frac{P_{18}(r_{i+1})}{P_{20}(r_{i+1})}\right) \tag{4}$$

The third method consisted of summing power estimates before ratios were taken, ie:

$$W_j{}^{(3)} = \frac{622}{2\Delta K \Delta R} \log_e\left(\frac{\Sigma P_{18}(r_i)}{\Sigma P_{20}(r_i)}\middle|\frac{\Sigma P_{18}(r_{i+1})}{\Sigma P_{20}(r_{i+1})}\right) \tag{5}$$

where

$$\Sigma \equiv \sum_{i=j-n}^{i=j+n} .$$

The final method consisted of processing the pulse to pulse ratios,

$$W_j^{(4)} = \frac{622}{2\Delta \, K\Delta R} \, \Sigma(R_i - R_{i+1}) \tag{6}$$

with Σ having same meaning as above and the R_i being summed over N pulse pairs, ie:

$$R_i = \sum^{N} \log_e(P_{18}(r_i)/P_{20}(r_i))$$

An expression for the mean square error of the estimates is given in Appendix IV.

The averaging methods (2), (3), and (4) are represented by a cross, a diamond and a triangular symbol respectively in the plots of smoothed differential attenuation versus range shown in subsequent figures. Method (1) is not considered in these plots, because this provides only a smoothing of the raw water vapour estimates, compared with the smoothing of absorption differentials provided by the other three methods.

For the purposes of computing water vapour content, method (4) was considered the most reliable as it should minimise non-stationary transmission and scattering effects of the atmosphere. This method is the one which will be used for comparison with radiosonde estimates.

6. ANALYSIS OF SOUNDER RESULTS

Up to the present time, sounder profiles have been obtained on three separate occasions. These will be covered in order of significance, rather than chronologically.

6.1 Results for 3/12/81

6.1.1 Sounder data

The early morning radiosonde flight from Adelaide Airport (0830 Central Standard Time (CST)) had a 12°C temperature inversion at 1 km with an associated drop out of moisture level. The water vapour content of the atmosphere was of the order of 6 g/kg up to a height of 1 km, then dried out to almost zero. Profiles are given in figure 8, together with associated profiles for:

(a) refractive index (defined in Section 7);

(b) dry refractive index (mixing ratio assumed zero);

(c) potential refractive index (temperature, pressure and mixing ratio adjusted for a pressure of 1000 mbars);

(d) potential temperature (temperature adjusted for pressure of 1000/mbars).

These conditions provided for the desired characteristic to test the sounders ability to detect a sharp discontinuity in water vapour content. The sounder was operated from 0947 to 1017 (CST) in the long pulse high power mode (Run 1) and from 1022 to 1054 in the short pulse, low power mode (Run 2). A sonde was released at the sounder site at 0950. The reduced profile is shown in figure 9. This profile is very similar to the earlier one observed at Adelaide Airport.

The long pulse backscattered power as function of range is shown in figure 10 for the R(18) and R(20) line pairs. The smoothed differential of the return (R(18)-R(20)) is shown in figure 11 for the different processing methods. The running means were computed over 11 adjacent points to minimise quantization effects. This will be further considered in Section 6.1.2.

The short pulse backscattered power and differential absorption results (figures 12 and 13) show a generally linearly increasing absorption difference up to 950 m. This is consistent with the fixed value of the water vapour content up to this height. The absorption difference then remains constant up to 1050 m, indicating a negligible water vapour content. At greater heights the absorption difference is degraded by a falling signal-to-noise ratio.

The long pulse differential absorption results (figure 11) illustrates the degrading effect introduced at short ranges (<500 m) by power from the tail of the pulse scattered back at ranges less than the gated range. However, at longer ranges the apparent increase in differential absorption is initially greater than predicted by the model described in Appendix III, and then flattens out abruptly at a height of 1100 m.

Although the flattening of the short pulse curve in figure 13 at around 1000 m is most likely to be due to the sharp reduction in water vapour content at this level, the same conclusion would not hold for the long pulse result in figure 11 (where the flattening effect commences at 1150 m). As shown in Appendix III, the long pulse (pulse length 300 m) differential absorption would be expected to continue to rise for some distance above the top of the water vapour layer, due to the contribution of the reflected power below the top of the layer. The explanation for the failure of the measured curve to follow this prediction can be found in figure 10, which shows the presence of enhanced backscattering in the region 800 to 900 m, just below the inversion. The effect of this is to increase the apparent gradient of the differential absorption in the layer, and immediately above the layer a flattening occurs. This is shown in Appendix IV by a computer simulation, employing the model of Appendix III with the addition of an aerosol layer.

6.1.2 Comparison with radiosonde profile

Figure 14 is a replot of the mixing ratio profile previously shown in figure 9, compared with the data from the short and long pulse sounder runs on 3/12/81. The short pulse sounder points show a layer terminating at a slightly lower level than the radiosonde profile and are significantly different from that curve, allowing for errors in each

estimate (rms error bounds are plotted). Profile points for the long
pulse sounding are not shown above 1100 m because they were considered
to be too seriously affected by the aerosol layer previously mentioned.
They have also been omitted at levels below 700 m because of the
severity of pulse tail effects in this region. To investigate the
source of the discrepancy between the short pulse and radiosonde
profiles a number of unsmoothed short pulse differential absorption
profiles were inspected. The profiles all exhibited the same
oscillatory character. This is evident in figure 15, where averaged
differential absorption values for each range cell are plotted, based on
processing method (4), together with a smoothed curve over 11 points.

The initial ascending section of the unsmoothed differential absorption
curve in figure 15 exhibits the undesired effects of quantization by the
A/D converter, manifested by a staircase appearance for the trace.
Unfortunately, this limits the range resolution obtainable for the water
vapour estimates, since they are given by the gradients of the
differential absorption.

6.2 Results for 3/11/81

6.2.1 Sounder data

The morning radiosonde flight at Adelaide Airport had an adiabatic lapse
rate up to 900 m (see figure 16), with a stable layer above this level.
The water vapour content was 4 to 5 g up to 800 m, with a dip at 1450 m,
then started increasing again above this level.

The lidar was operated in long pulse and short pulse modes between 1016
and 1102 CST. The averaged backscattered power levels returned for the
R(18), R(20) line pair in the short pulse and long pulse modes are shown
in figures 17 and 18. The latter diagram shows the presence of cloud at
3400 m altitude with a 12.5 dB differential between the two lines at
this height. The differential absorption results are plotted in
figures 19 and 20. A switching transient in the input to the A/D
converter is evident in both plots, in the range interval
3750 to 4250 m. This transient is due to the A/D converter being
switched to the monitor detector, to record the level of the laser
pulse.

The rapidly climbing section of the long pulse curve (figure 20) is
again due to a reduction in the decay rate of the aerosol density at
about 700 m, which is evident from the backscattered power versus range
in figure 18. However, this layer has a much greater thickness
(extending to approximately 1400 m) than was exhibited by the aerosol
layer present in figure 10.

6.2.2 Comparison with radiosonde profile

The profile comparison is made in figure 21. The long pulse profile is
in reasonable agreement above 800 m, with lower altitude estimates
seriously affected by the long pulse tail effect. The spuriously high
value of the mixing ratio at 700 m is probably due to the appearance of
an aerosol layer at about this height. The error bars in figure 21 are
generally greater than for figure 14 because the backscattered power
showed a wider fluctuation on this occasion. The smoothing procedure
employed on all profiles has removed much of the oscillatory component
(thought to be due to quantization noise), which is also particularly
noticeable in other short pulse profiles.

6.3 Results for 24/11/81

6.3.1 Sounder data

Three sounder runs were performed on this day, runs one and two using
the long pulse mode commencing at 1002 and 1033 CST respectively, and a
short pulse run starting at 1112 CST.   The DRCS radiosonde profile was
obtained at 1112 CST.   Since the two long pulse runs, consisting of 54
and 61 pulse pairs respectively, gave very similar results it was
decided to combine the two runs together to form a single data set. The
backscattered power and differential absorption plots for the long pulse
run are shown in figures 22 and 23 respectively.   The absorption
difference variation with range shows three characteristic regions. The
initial low gradient section is again due to the pulse tail effect. The
rapidly climbing section is due to a reduction in the decay rate of the
aerosol density at about 800 m.   This layer extends up to
1300 to 1400 m.   The evidence for this is found in the average
backscattered power versus range results of figure 22.

6.3.2 Comparison with radiosonde profile

The resulting profile in the region 600 m to 1300 m is shown in
figure 24, together with the corresponding radiosonde profile.   The
higher values of mixing ratio, relative to radiosonde values, obtained
between 700 to 900 m, are again due to the influence of the aerosol
layer mentioned above.

The short pulse results are shown in figures 25 and 26.   The
differential absorption measurement (figure 26) is limited by signal-to-
noise restrictions above 750 m.   The oscillatory component, arising from
quantization noise, has been removed from the lower altitude section of
the short pulse profile of figure 26 by smoothing, as for the two
previous cases considered in Sections 6.1.1 and 6.1.2.

6.4 Effect of signal-to-noise degradation on layer determination

It is apparent in the plots of differential absorption versus range, that
all curves monotonically increase at lower heights, when there is good S/N
ratio, and eventually begin descending as the S/N ratio falls below the
absorption differential.   Care, therefore, must be exercised to avoid
interpreting a reduction in S/N ratio as a decrease in water vapour
content.   Water vapour estimates were only calculated in the plots of
figures 14, 21 and 24 when the signal-to-noise of the weaker return was
above a value of approximately 10 dB.   Using power samples with S/N ratios
below this value will lead to serious errors.

An illustration of this point is provided by the differential absorption
curve of figure 26 which has a plateau above 750 m altitude. As previously
discussed, this is usually indicative of a very low water vapour content.
However, in this case inspection of the backscattered power return
(figure 25) shows that at the plateau base height (6750 m) the S/N ratio of
the R(20) return was less than 10 dB, with evidence of corruption by noise.
Hence the differential absorption curve was not used for water vapour
content estimation in this region.

7. FUTURE DEVELOPMENTS

7.1 Increase in sampling resolution

As discussed in Section 6.1.1 the resolution obtainable for water vapour
estimates was limited by the six bit A/D converter.   This converter is
presently being replaced by an eight bit device and it is anticipated that
this will significantly improve the resolution and accuracy of the
estimates.

7.2 Improvements to signal-to-noise performance

7.2.1 Heterodyne detection

Heterodyne detection improves the signal detection threshold by several
orders of magnitude over direct detection.   This can be implemented by
using a separate local oscillator which beats with the backscattered
energy and the transmitter to produce two rf signals whose difference
can be controlled by a loop.   The difference signal is then envelope
detected to give the amplitude(ref.6).   A further possible advantage to
be gained is the rejection of the tail of the laser pulse by the loop
filter since the decaying part of the pulse exhibits a changing
frequency shift.

7.2.2 Background limited detection

At present the limiting noise in the detection system arises from the
front end of the preamplifier (noise figure 4 dB).   It may be possible
to reduce the amplifier noise level so that the background sky noise
becomes the limiting noise.   Further noise reduction would then be
possible by using an optical filter.

8. CONCLUSIONS

The infra-red tunable sounder is capable of measuring water vapour profiles to
at least 1.5 km, but the height capability is dependent on the atmospheric
aerosol distribution.   In cases of strong temperature inversions, the aerosol
density often builds up below the inversion and then falls off rapidly above
the inversion.   This can lead to serious distortion of the differential
absorption estimates for long pulse transmissions.   However, for short pulse
emissions the range capability of the lidar may be improved (as in the case of
the measurements on 3/12/81 due to the increase in the intensity of the return
from below the inversion level.

The results in this paper show the necessity of using a short pulse emission
in the presence of atmospheric inversions   to enable the features of
atmospheric water vapour layers to be resolved.   The data presented show that
the sounder is capable of profiling in the height range where radio ducts are
most frequent(ref.7),   and most seriously affect surface based radio frequency
sensors and communications systems. Further development and refinement of the
sounder S/N performance is required to utilize to the full its undoubted
potential, which could rival the radiosonde in accuracy.

ERL-0230-TM   - 12 -

9. ACKNOWLEDGEMENTS

I am indebted to the following ERL staff members who assisted during the
project: Mr N. Bromilow and Mr D. Anderson for the design and construction of
the telescope and optical system; Mr J. Silby and Mr J.C. Crombie for the
design and construction of the microprocessor-based recording system and
installation of the detector; Mr R. Keough for initial assembly of the lidar,
design and construction of components, and assistance with the optical
alignment work; and Mr M. Rawolle for advice.

REFERENCES

No.	Author	Title
1	Schotland, R.M.	"The Determination of the Vertical Profile of Atmospheric Gases by Means of a Ground-Based Optical Radar". Proc. Third Symposium on Remote Sensing of Environment, Ann Arbor, 1964
2	Browell, E.V., Wilkerson, T.O. and McIlrath, T.J.	"Water Vapour Differential Absorption Lidar Development and Evaluation". Applied Optics 18 3474, 1979
3	Asai, K., Itabe, T. and Igarashi, T.	"Range-Resolved Measurements of Atmospheric Ozone Using a Differential Absorption CO_2 Laser Radar". App. Phys. Lett. 35 p60, 1979
4	Murray, E.R., et al	"Atmospheric Water Measurements with an Infra-Red (10-μM) Differential Lidar System". App. Phys. Lett. 28 542, 1976
5	Shumate, M.S., Menzies, R.T., Margalis, J.S. and Rosengren, L.G.	"Water Vapour Absorption of Carbon Dioxide Laser Radiation". Applied Optics 15 2480, 1976
6	Lundquist, S., Falt, C.O., Persson, U., Mathinsson, B. and Eng, B.T.	"Air Pollution Monitoring with a Q-Switched CO_2 Laser Lidar using Heterodyne Detection". Applied Optics, Vol. 20 No. 14, 1981
7	Baker, P.W. and Dowd, A.M.	"The Occurrence of Radio Ducting, Superrefractive Subrefractive Conditions in Australian Maritime Regions". ERL Tech Report ERL-0048-TR, November 1978
8	Crombie, J.C.	"An Infra-Red Sounder for Measurement of Water Vapour Differential Absorption in the Atmosphere". ERL Tech Memorandum (in publication)

TABLE 1.   RESULTS OF DIFFERENTIAL ABSORPTION MEASUREMENTS

Reference	Molecule	Wavelength (μm)	Path Direction	Resolution (m)
* Bowell et al (1979) (ref.2) NASA	H_2O	0.7243	Vertical	100
Asai,Itabe, Igarashi (1979) (ref.3) RRL Japan	O_3	10.6	Horizontal	500
Murray et al (1976) (ref.4) SRI	H_2O	10.6	Horizontal	30
Schotland (1964) (ref.1)	H_2O	0.6943	Vertical	300

*Simultaneous transmission on two laser wavelengths.

TABLE 2. CO_2 SOUNDER SYSTEM PARAMETERS

CO_2 TEA Laser	
Transmitted Energy	
(a) Maximum	4 J
(b) Without N_2 in gas mix	0.1 J
Lines	R(18), R(20), R(22) on 10 μm band
Pulse Width	
(a)	1 μs (to e^{-1} level)
(b)	100 ns (to e^{-1} evel)
Beam Divergence	1 x 0.6 mrad
Typical PRF	0.07 Hz
Maximum PRF	0.5 Hz

Receiver	
Telescope diameter	30 cm
Field of view	1 mrad FWHM
Hg-Cd-Te photoconductive detector D*	3×10^{10} cm Hz /W
Time Constant	50 ns
Size	1 x 1 mm
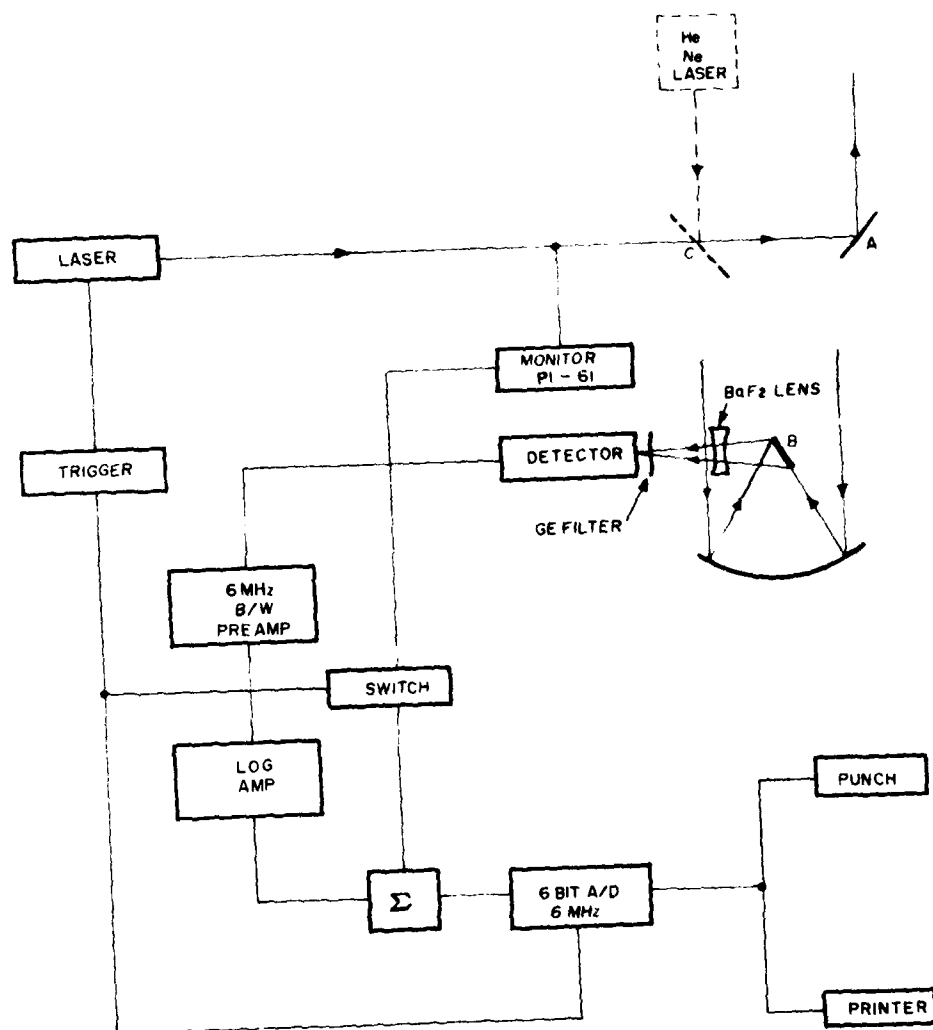
Figure 1. Block diagram of LIDAR and recording system
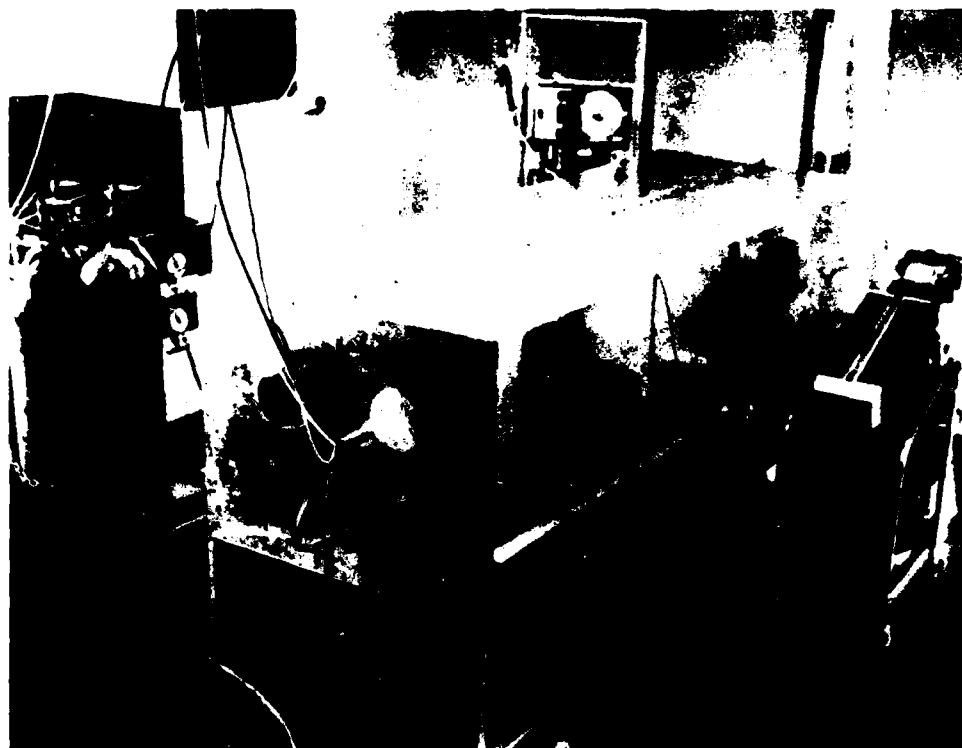
Figure 2.   Aluminium screen constructed to double-shield laser from detector
            and recording electronics
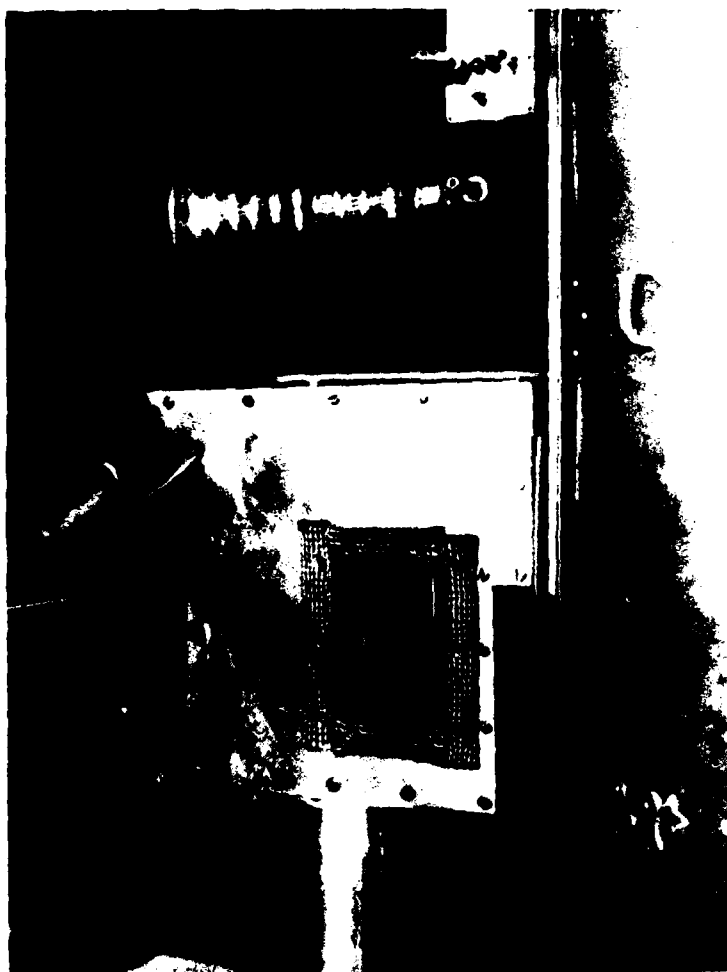
Figure 3. Double shielding enclosure for detector
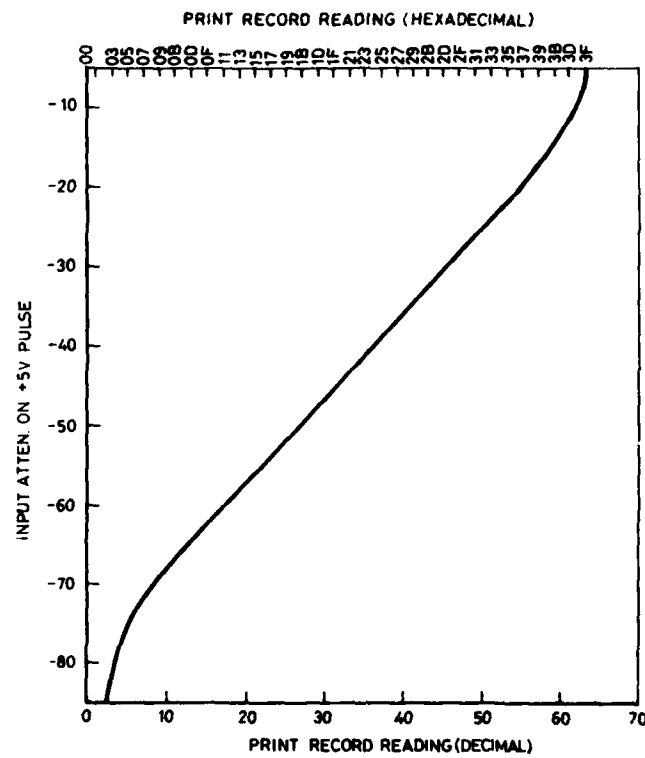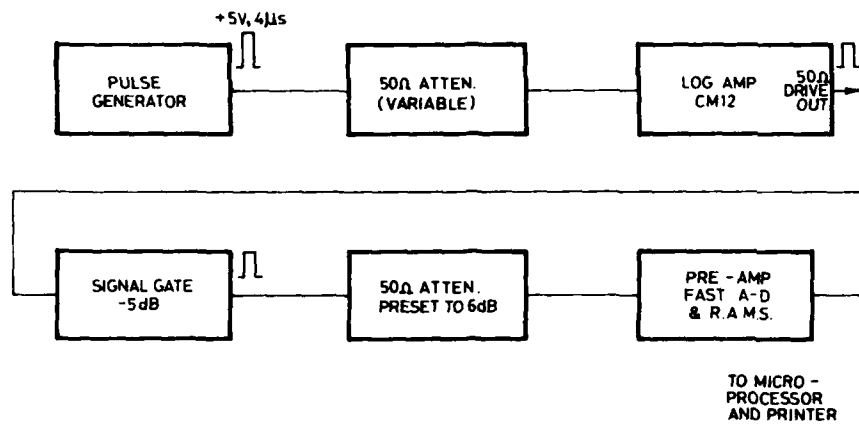
Figure 4.   Laser signal processing calibration

Figure 5.   Hills face area used for target
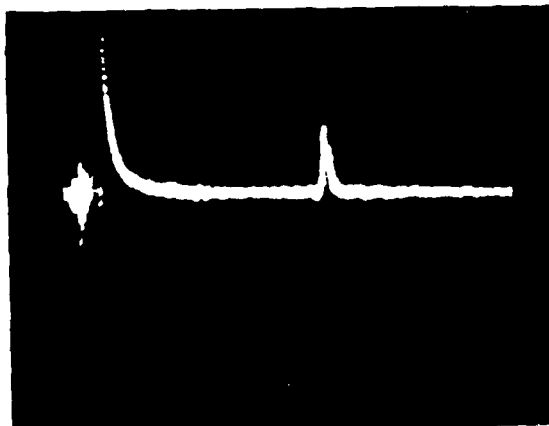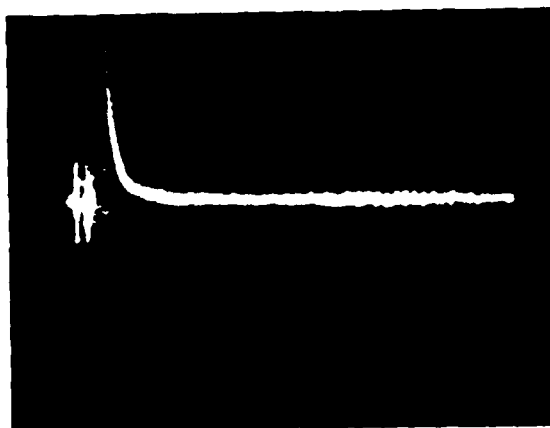
Figure 6.   Echoes from hills face at three different CO_2 transmission lines
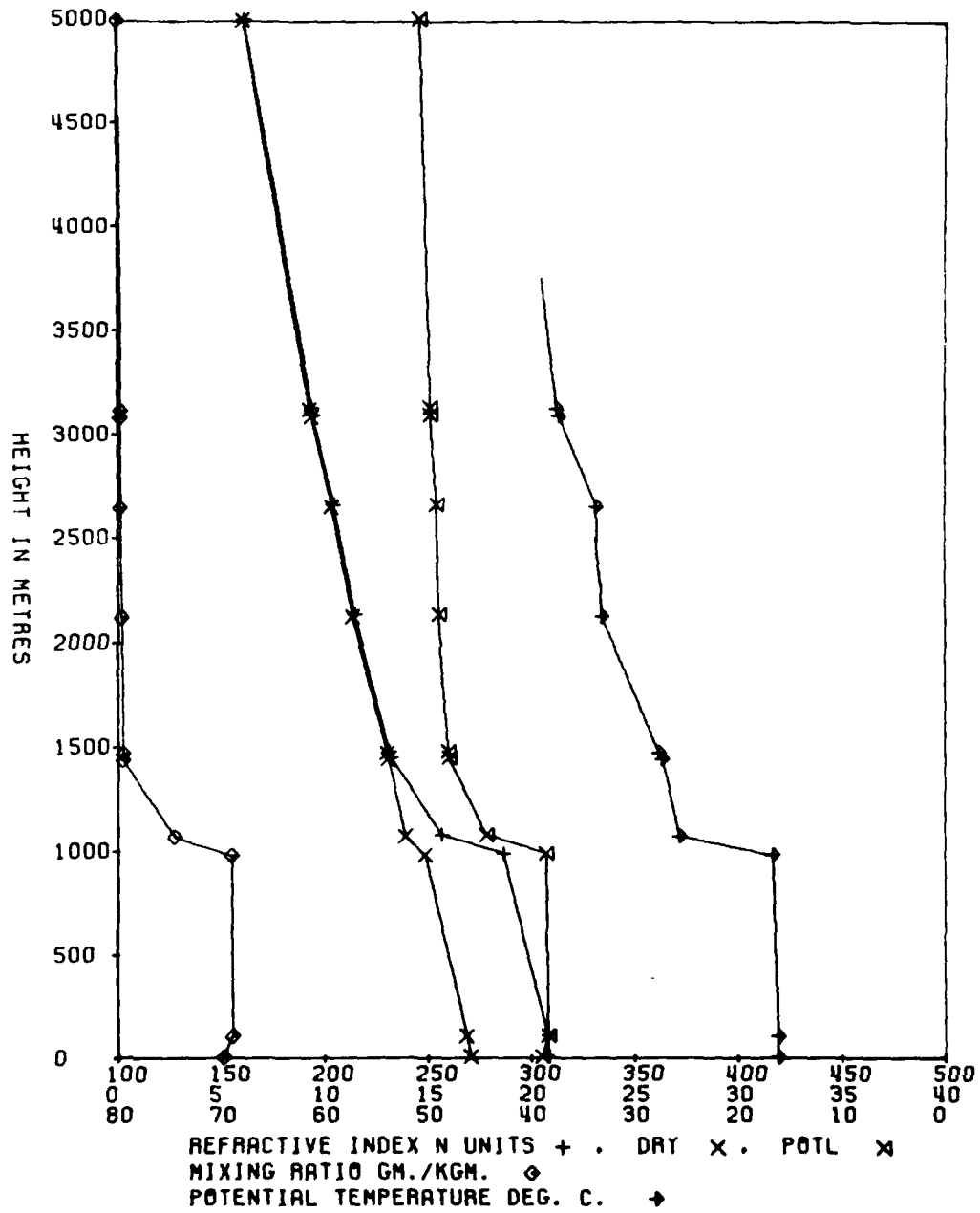(a) R(18), (b) R(22), (c) R(20)
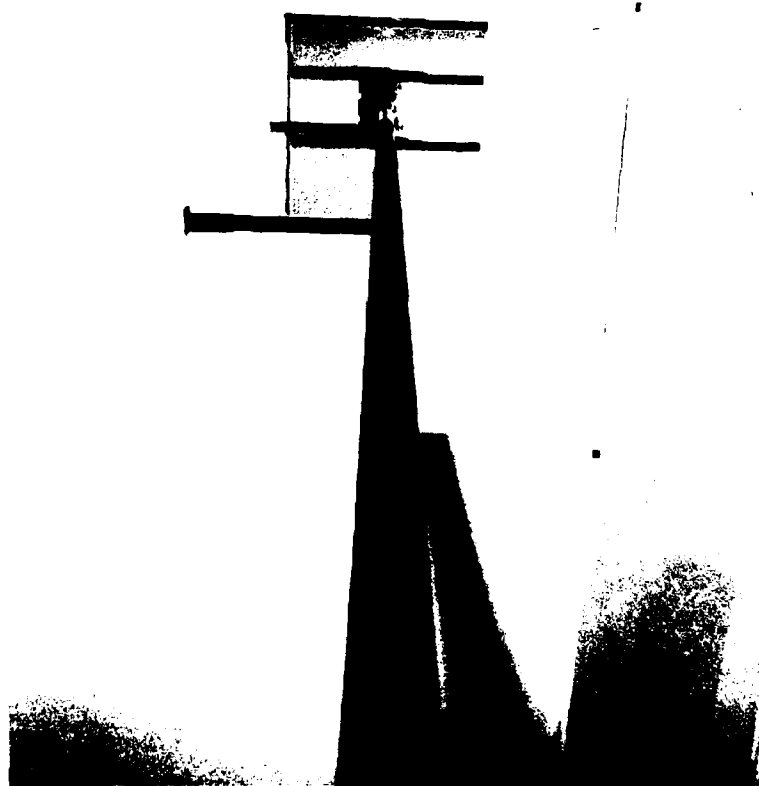
Figure 7. Vertical pipe to enclose laser beam inside building

Figure 8. Adelaide Airport radiosonde profiles 0830 CST, 3-12-81
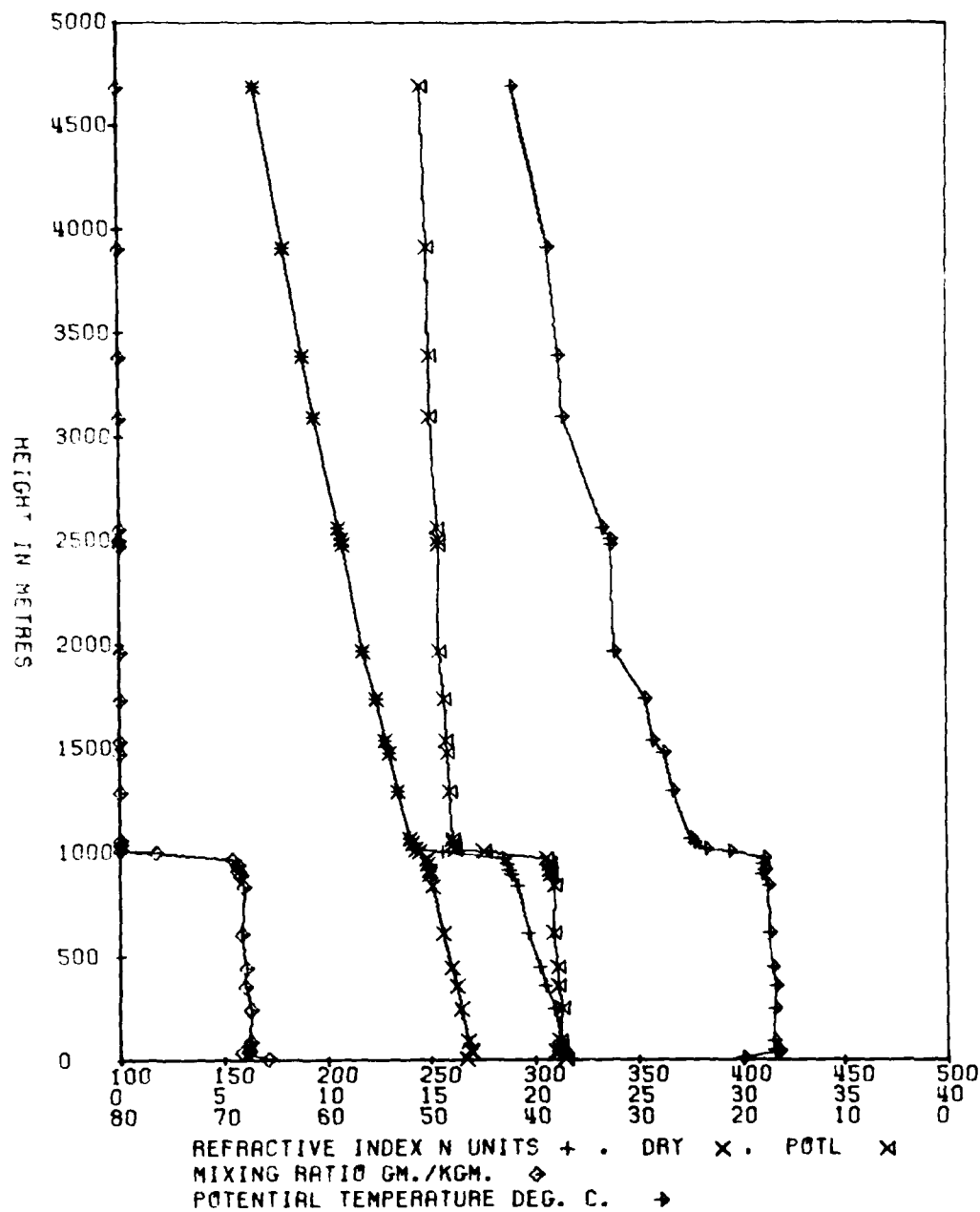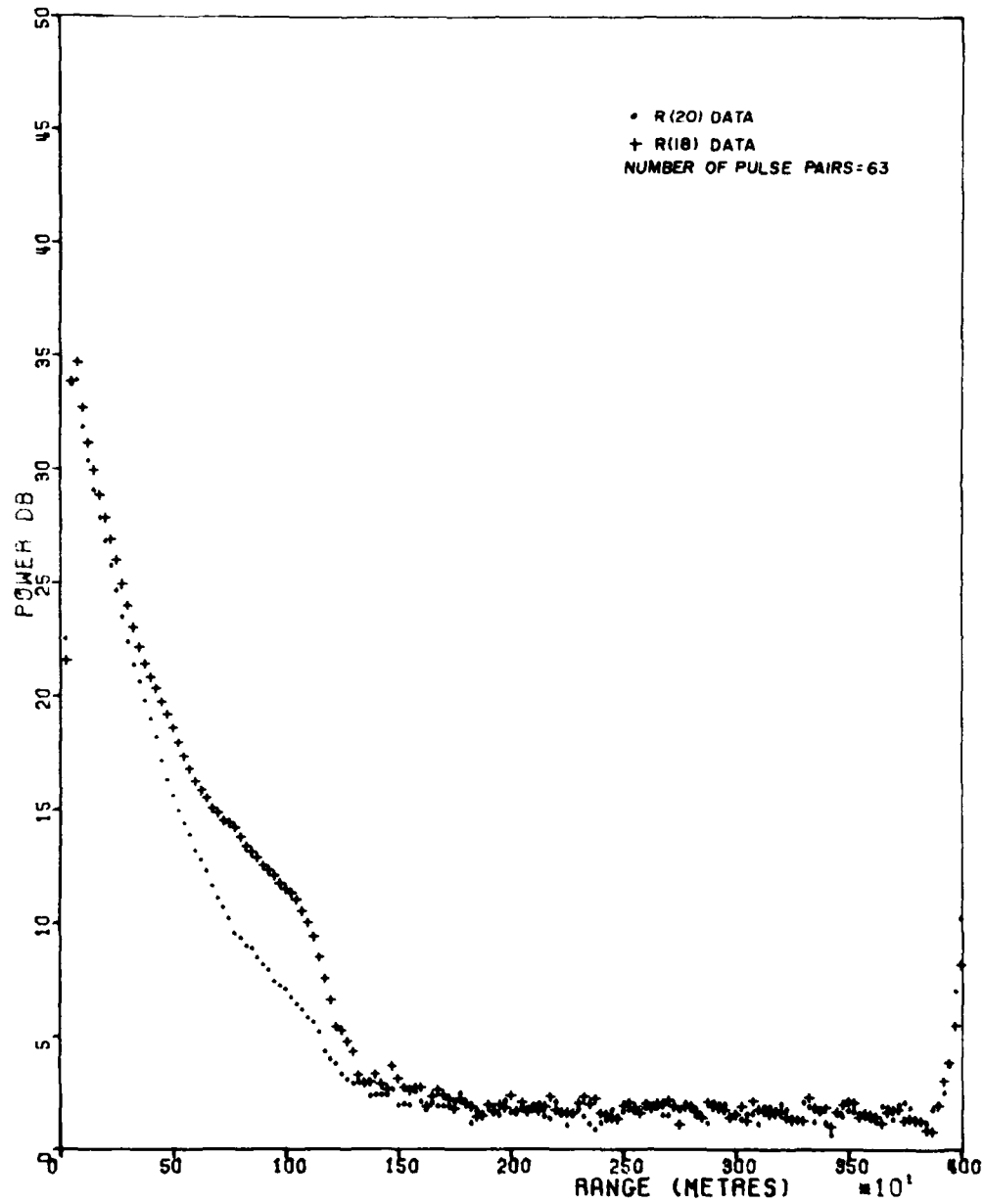
Figure 9.   DRCS radiosonde profiles 0900 CST, 3-12-81
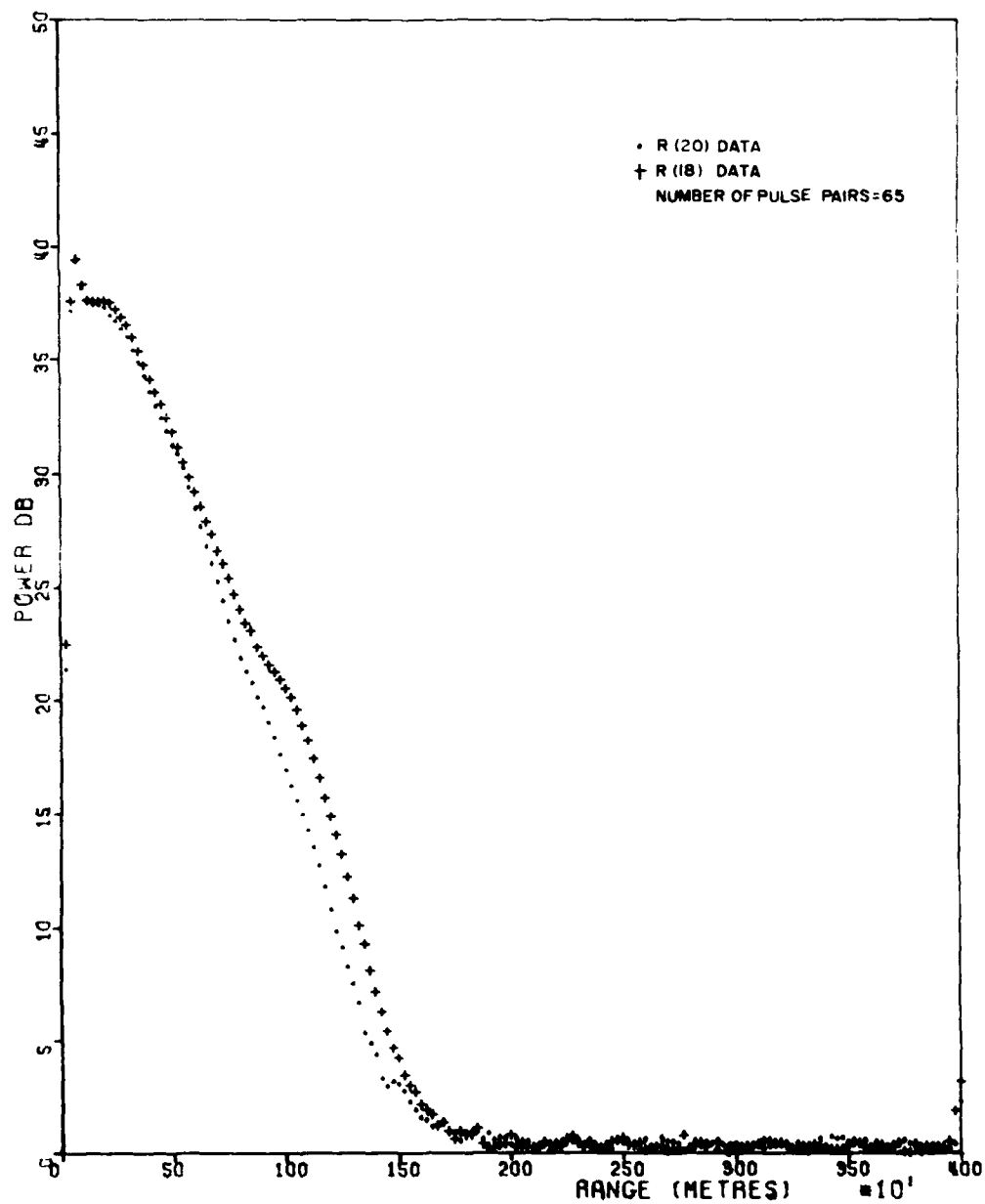
Figure 10. Returned power versus range for long pulse run (at 0947 CST) on
3-12-81, for R(20) and R(18)
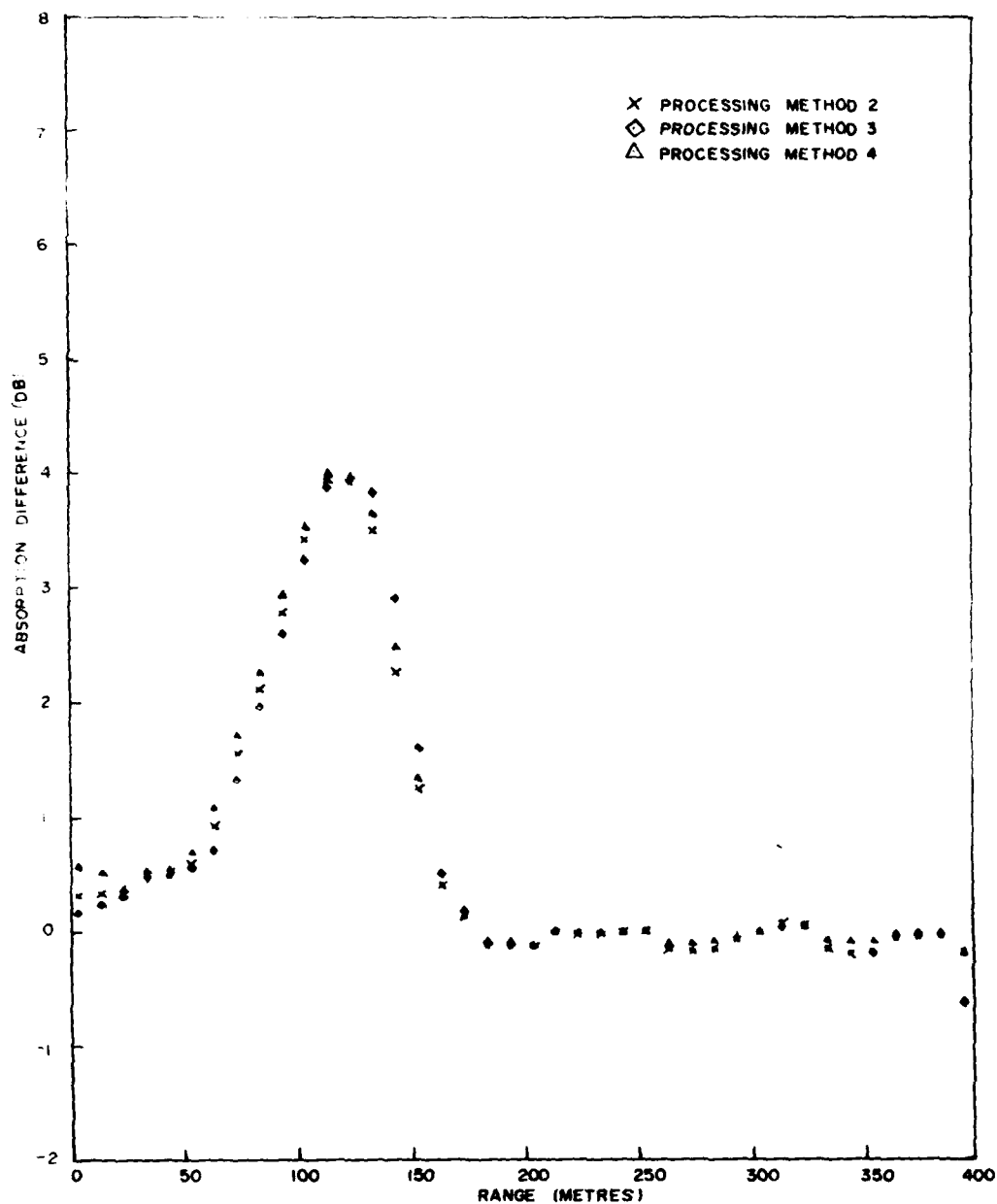
Figure 11. *Differential absorption versus range for long pulse run 3-12-81*

Figure 12. Returned power versus range for short pulse run (at 1022 CST) on
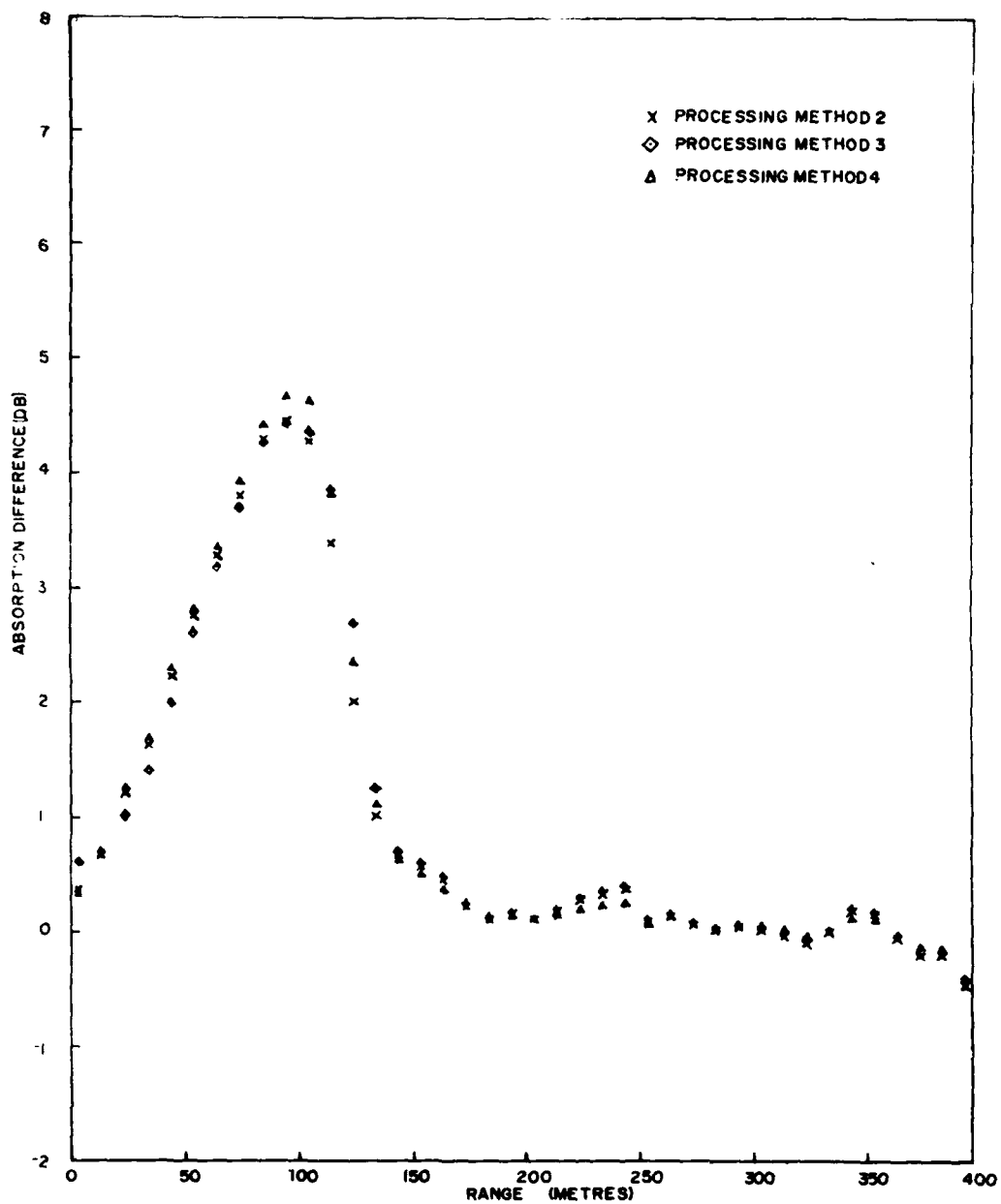3-12-81, for R(20) and R(18)

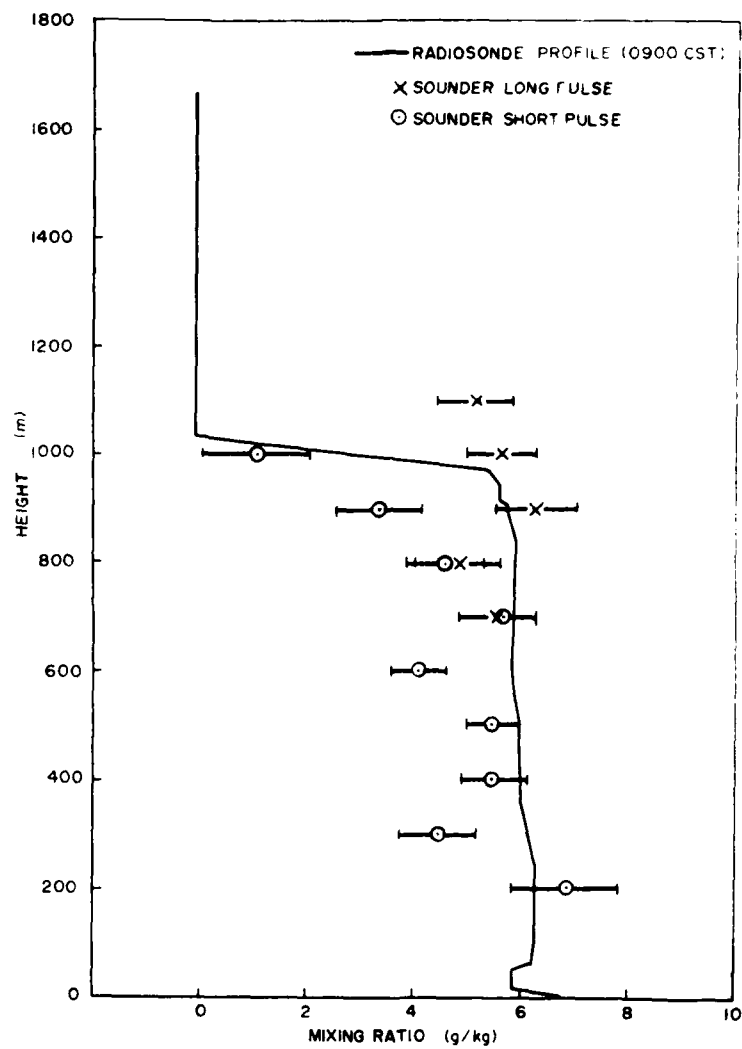Figure 13. Differential absorption versus range for short pulse run 3-12-81

Figure 14. Water vapour data from long pulse and short pulse soundings for
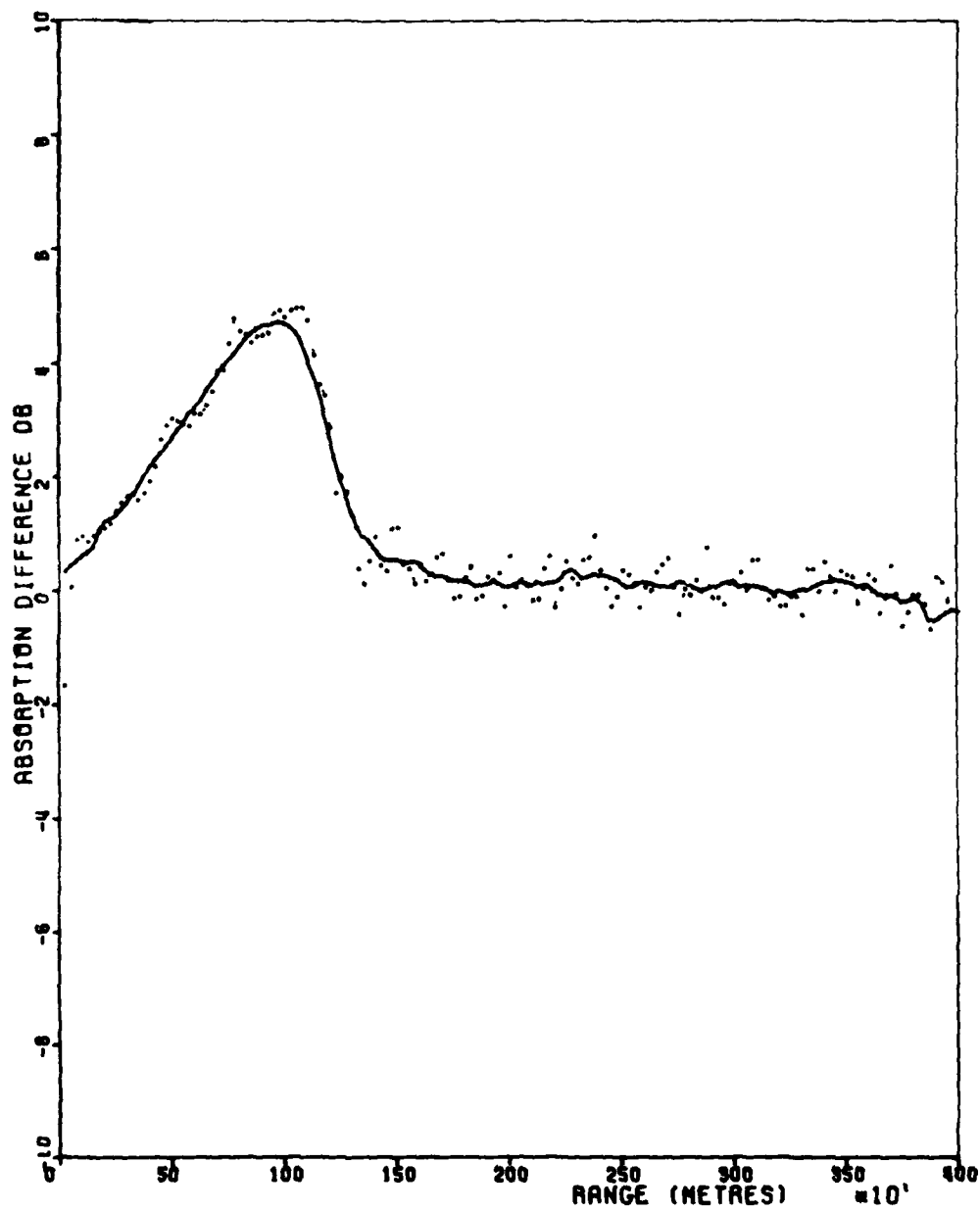period 0947-1057 CST on 3-12-81

Figure 15. Average 25 m range cell differential absorption data for short
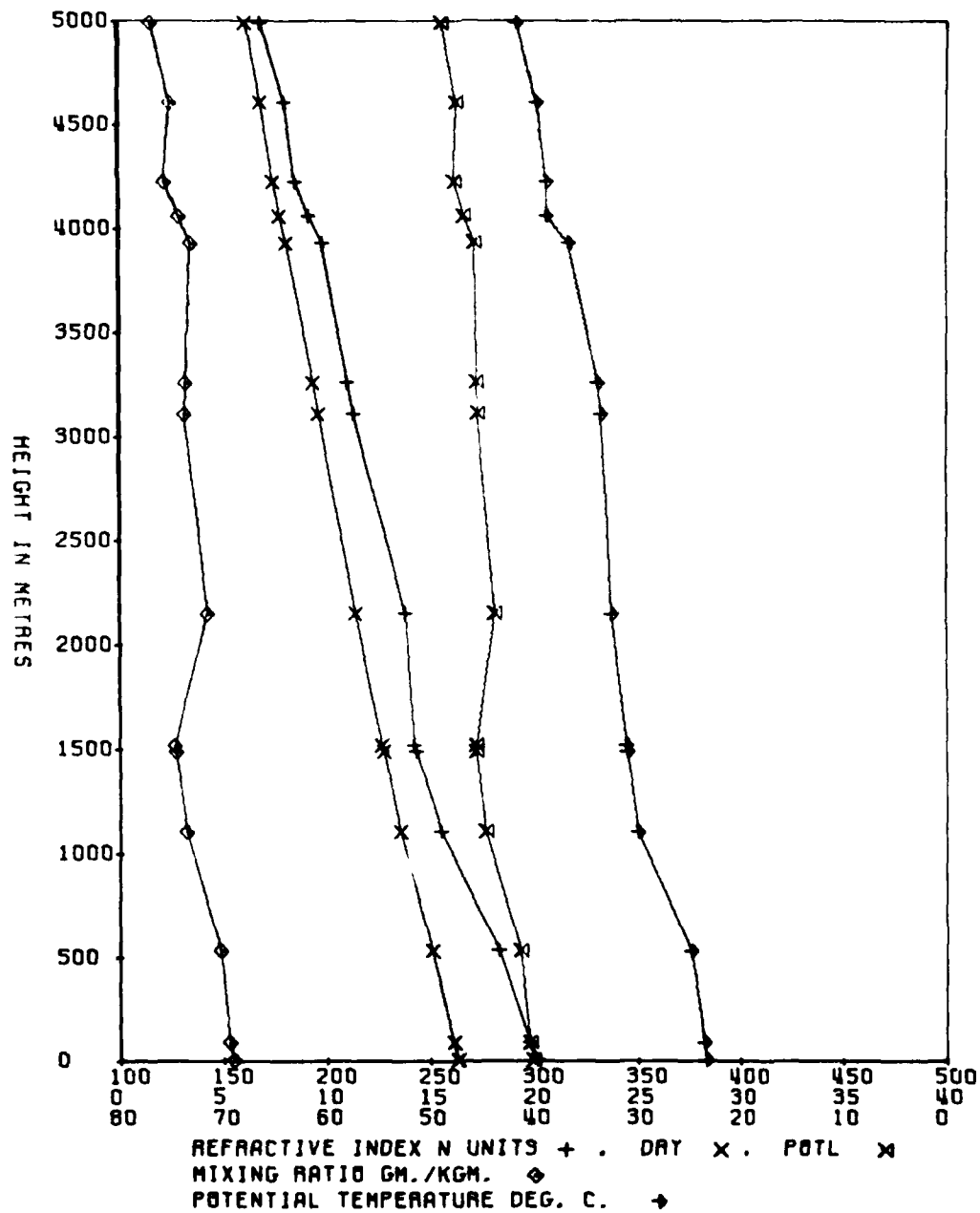   pulse run on 3-12-81

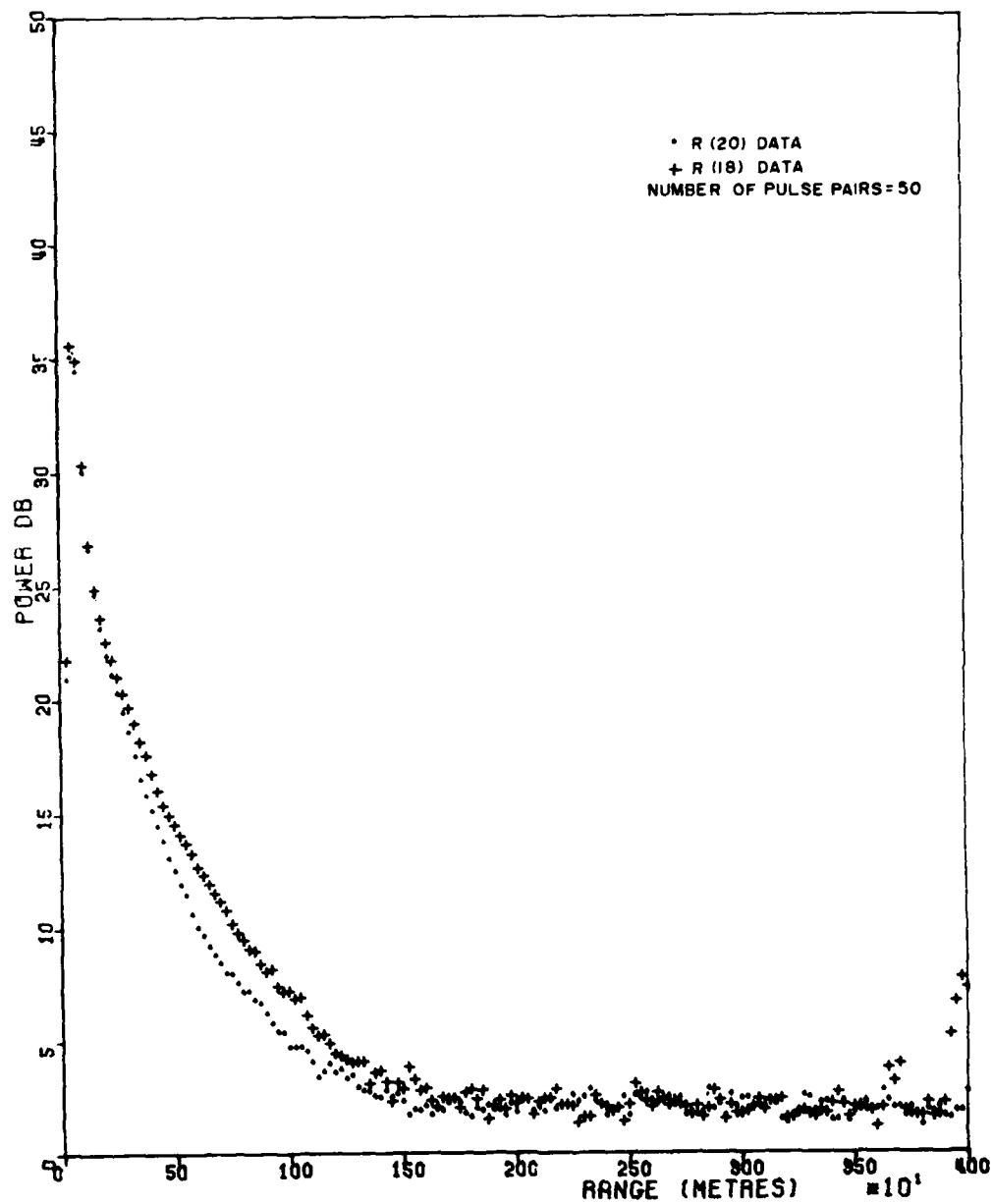Figure 16. Adelaide Airport radiosonde profiles 0830 CST, 3-11-81

Figure 17. Returned power versus range for short pulse run (at 1016 CST) on
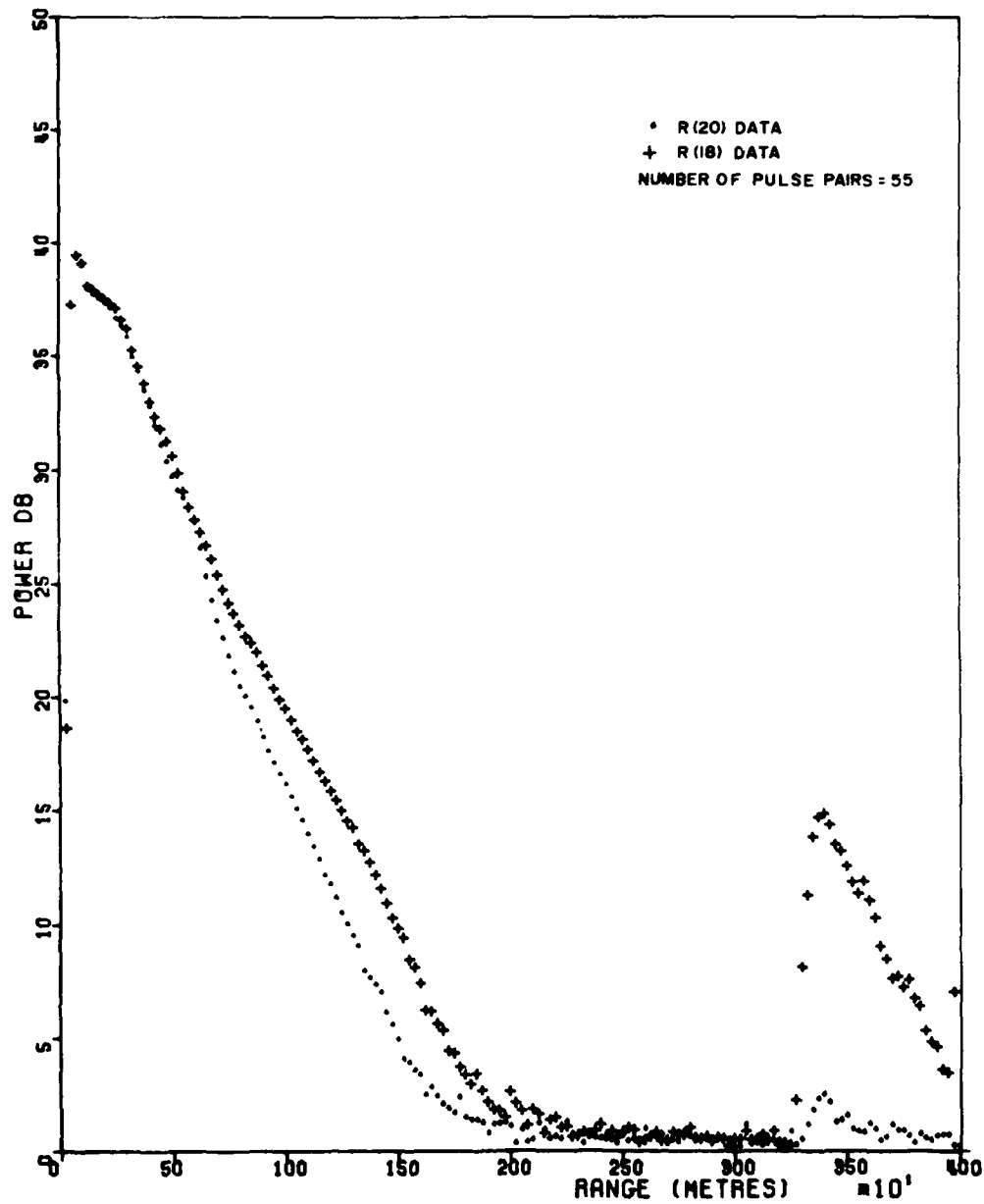3-11-81 for R(20) and R(18)

Figure 18. Returned power versus range for long pulse run (at 1108 CST) on
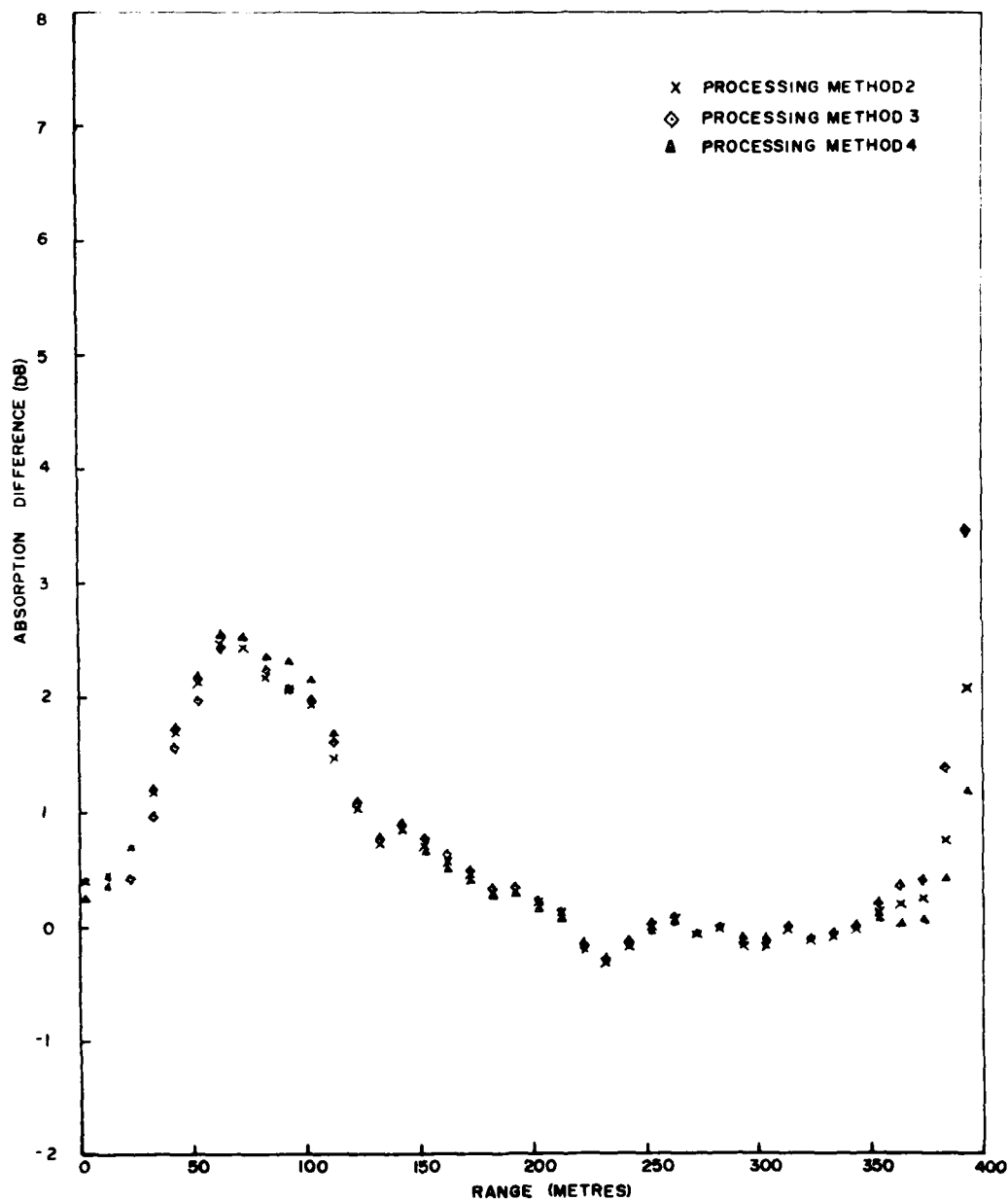3-11-81 for R(20) and R(18)

Figure 19. Differential absorption versus range for short pulse run on 3-11-81

Figure 20. Differential absorption versus range for long pulse run on 3-11-81

Figure 21. Water vapour data derived from long pulse and short pulse soundings
for period 1016 to 1145 CST on 3-11-81

Figure 22. Returned power versus range for long pulse run (at 1002 CST) on
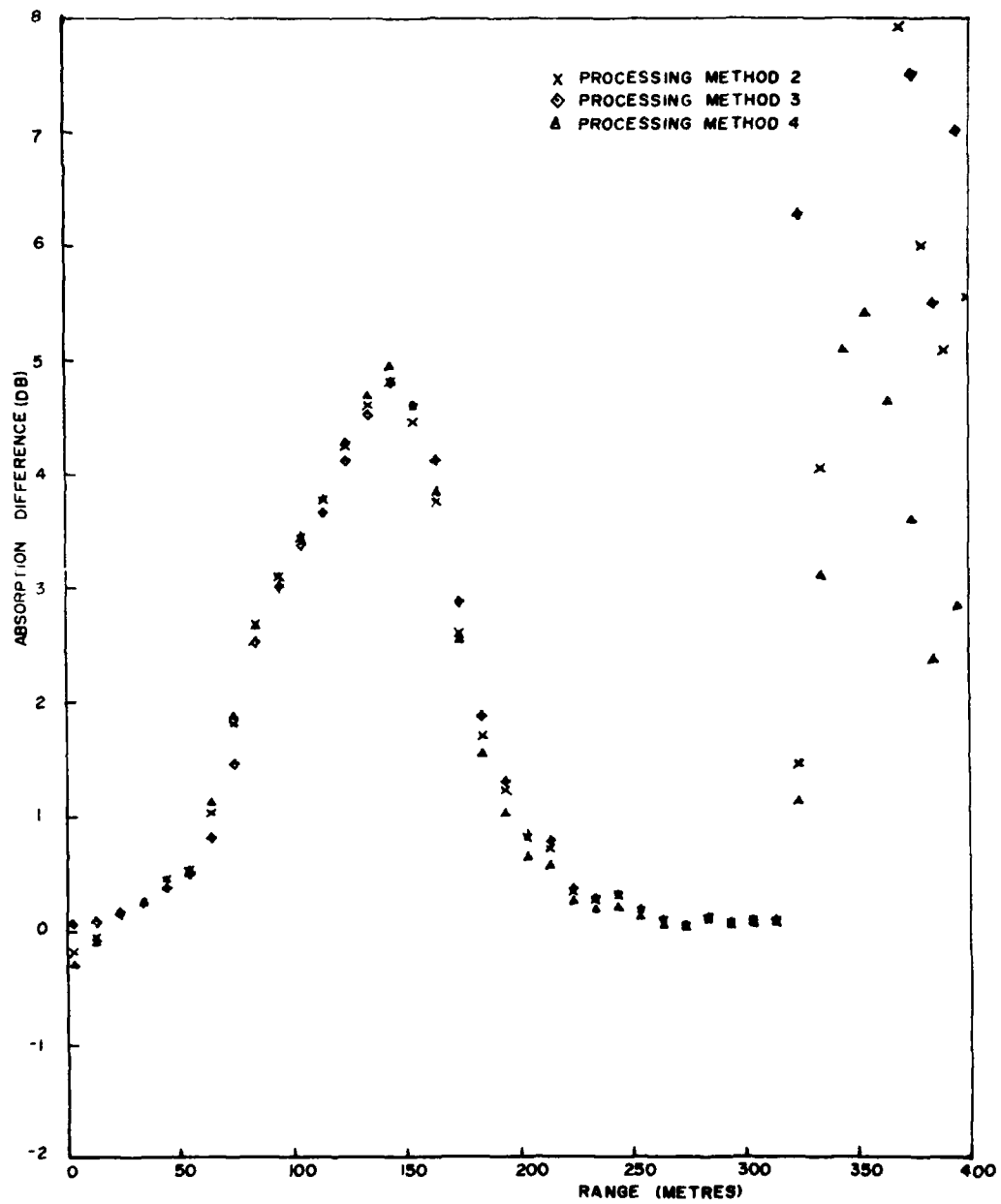24-11-81, for R(20) and R(18)

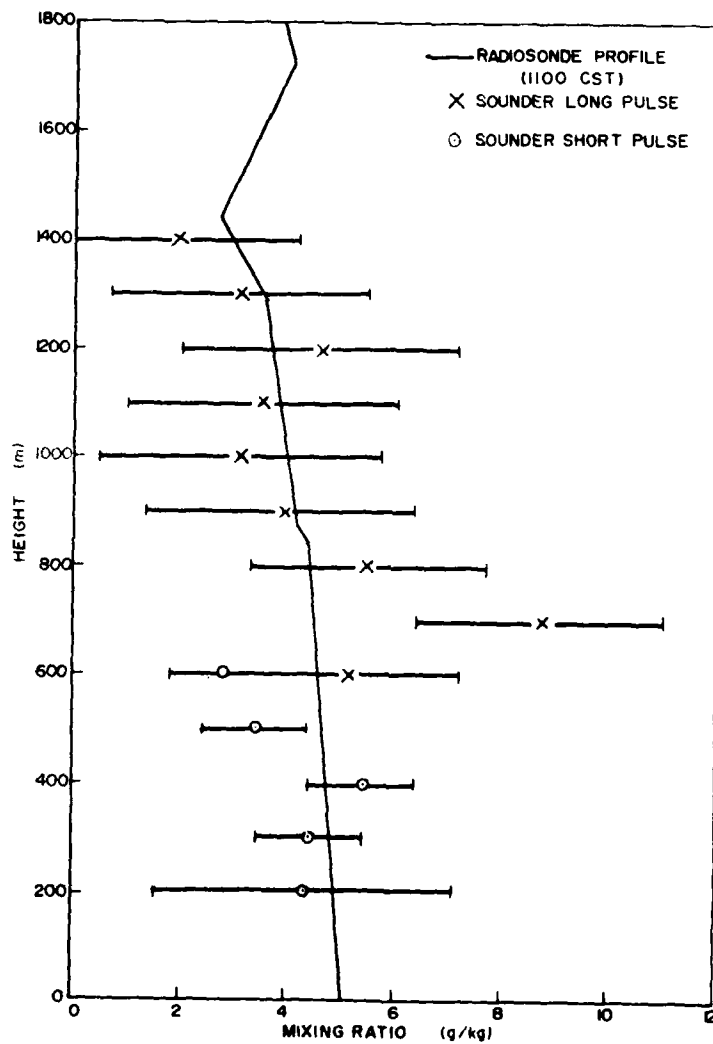Figure 23. Differential absorption versus range for long pulse run on 24-11-81

Figure 24. Water vapour data derived from long pulse and short pulse soundings
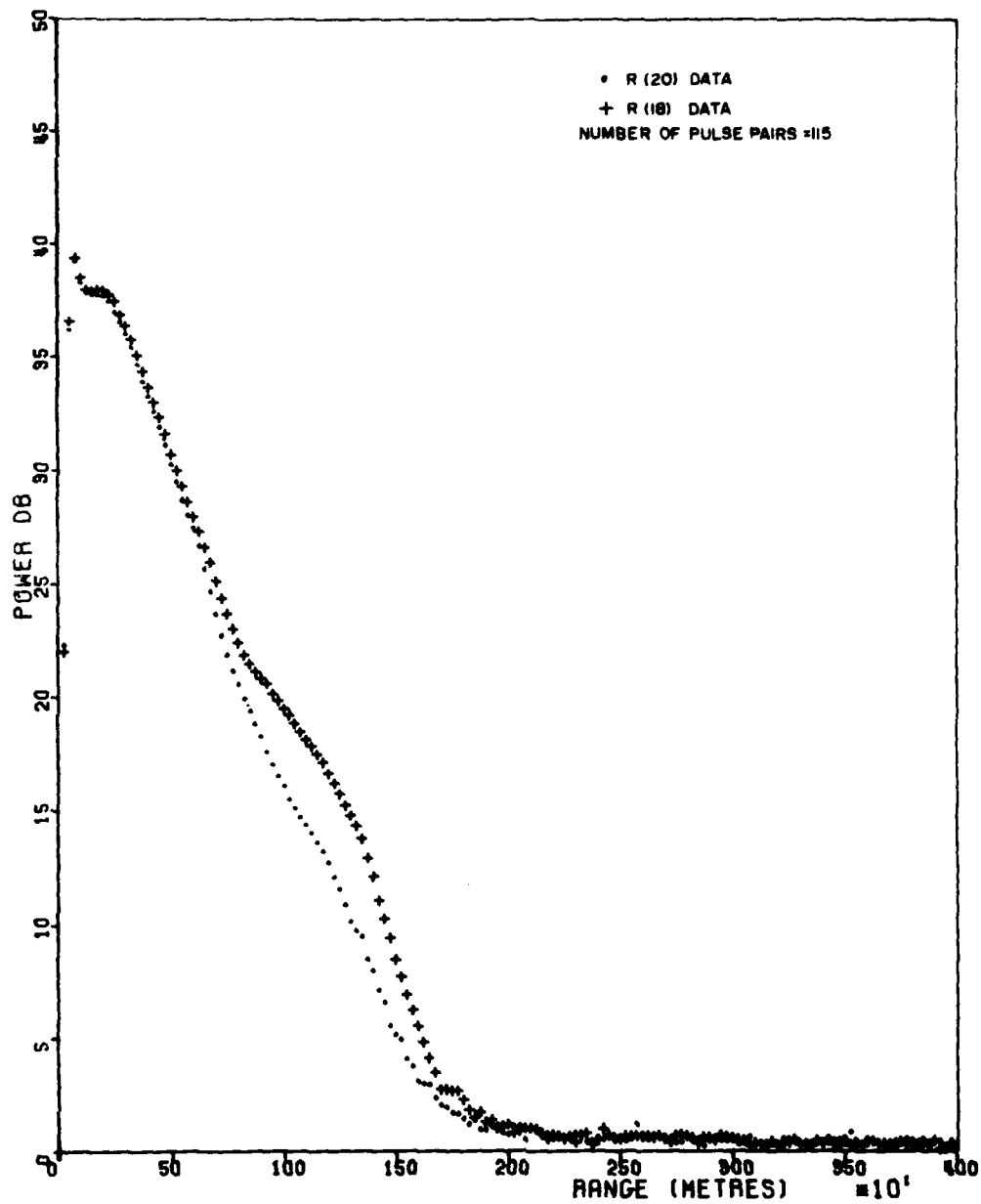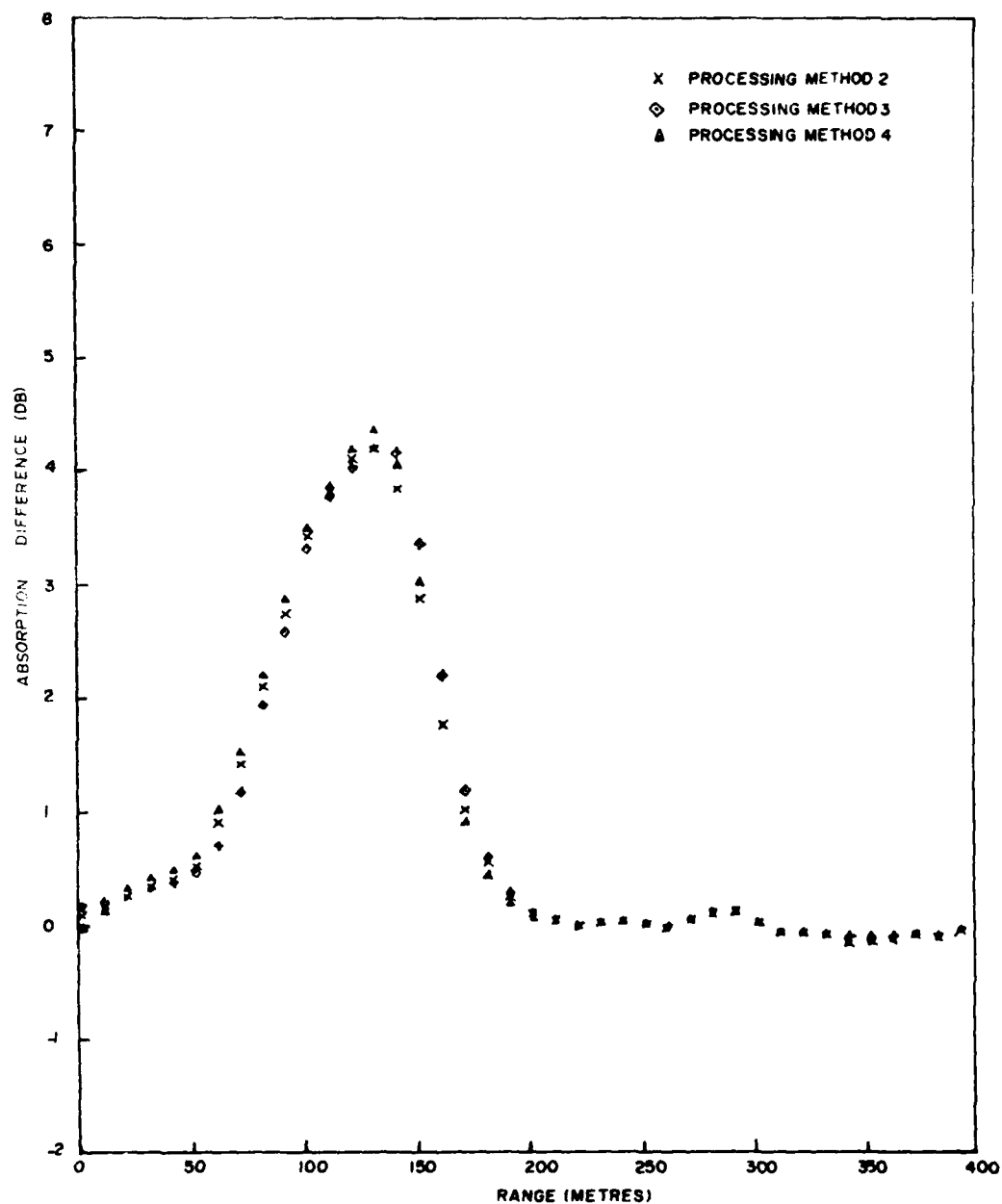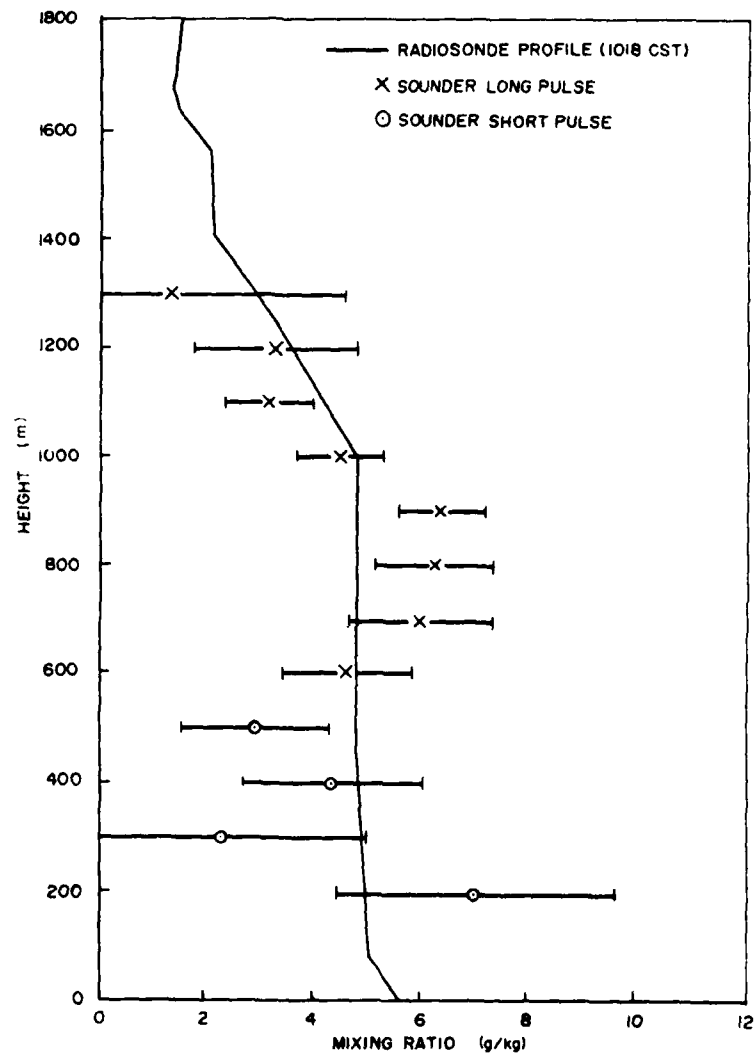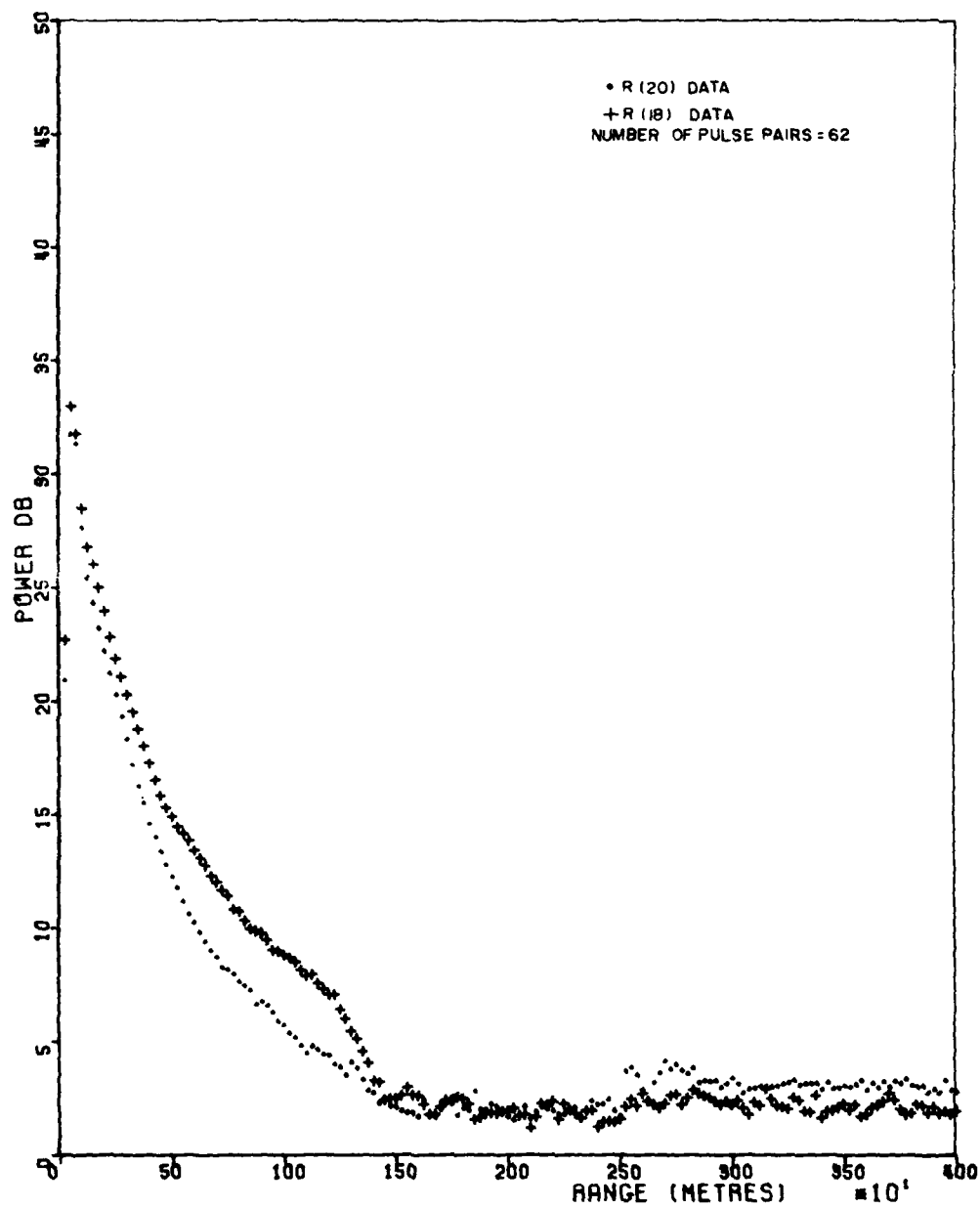for the period 1002 to 1138 CST on 24-11-81

Figure 25. Returned power versus range for short pulse run (at 1112 CST) on
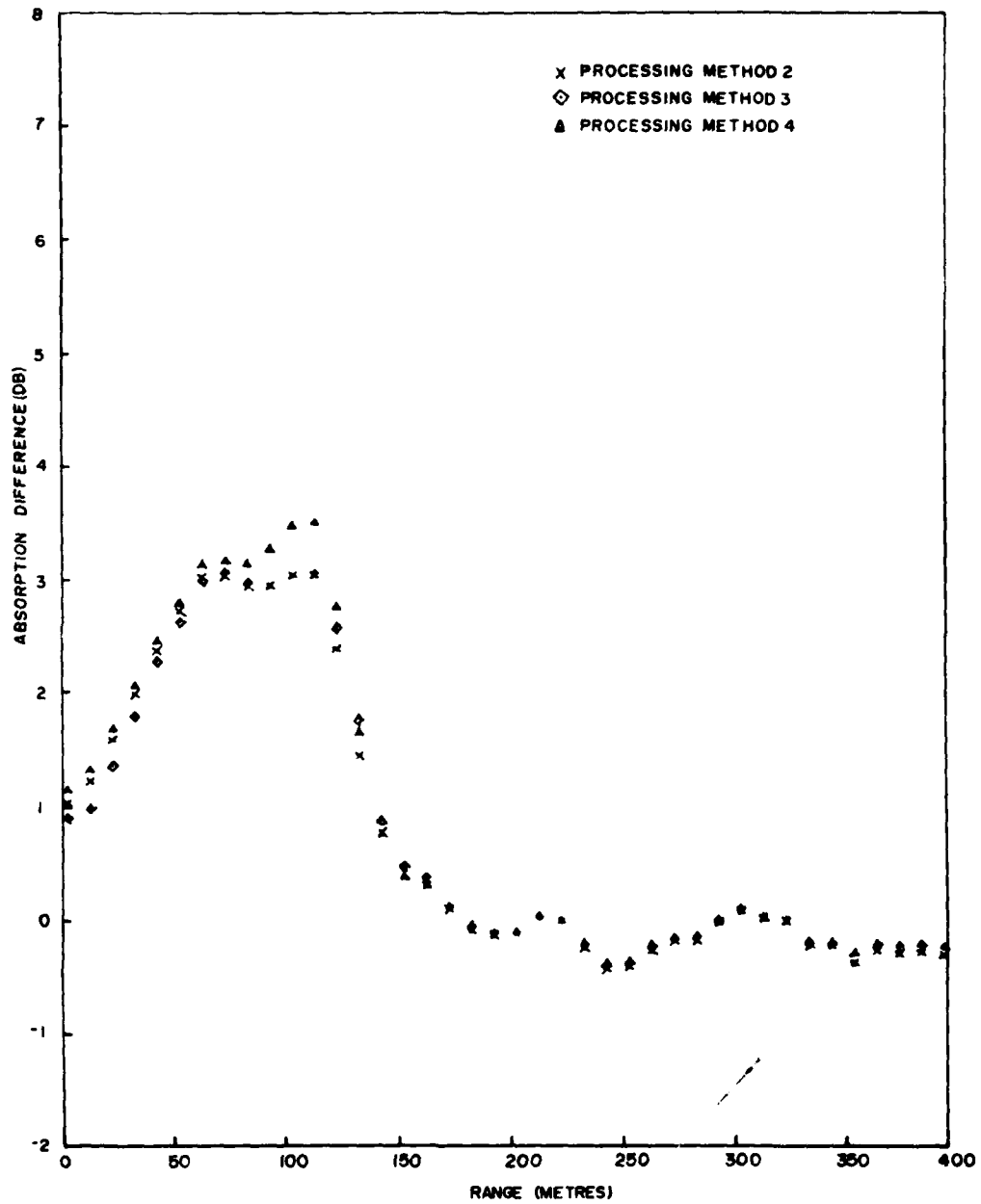24-11-81, for R(20) and R(18)

Figure 26. Differential absorption versus range for short pulse run on
24-11-81

APPENDIX I

OPTICAL ALIGNMENT PROCEDURES

I.1 Approximate method

The Newtonian telescope is designed to image on a detector mounted on the side of the telescope. The assembly holding the 45° telescope mirror B and a focussing lens, also houses the 45° mirror (hereafter called laser mirror A) which deflects the beam from its initial horizontal path to a vertical trajectory.

A helium neon (HeNe) laser is substituted for the CO_2 laser by interposing a mirror C at 45° along the patch between the laser and laser mirror A. The HeNe beam is brought in from the side, as indicated by the dashed line in the figure.

The Newtonian telescope is aligned relative to the reference HeNe laser beam by the following technique:

(i)   A reference transmission beam line is established (using the HeNe laser), which after reflection from mirror A passes through the centre of the roof aperture. The reference beam is centred on a chosen position in the plane of the roof opening by adjusting laser mirror A. This is the only adjustment for which this mirror is employed.

(ii)   The telescope is then aligned to this reference by using a retroreflector to reflect the reference ray back into the telescope and rotating the retroreflector through 360° to generate a cylinder of returning rays (in temporal sequence).   The axis about which the cylinder of rays is focussed is adjusted, by means of mirror B, to pass through the centre of the detector.   (The HeNe focussing image is displaced 171 mm beyond the position of the CO_2 focussing plane because of the wavelength dispersion characteristic of the focussing lens.)

(iii)   The HeNe laser is then removed and CO_2 laser brought into alignment with the reference line.

This is not a precise procedure because it relies on centering the CO_2 laser beam on the 260 mm length light tube (45 mm diameter) leading to laser mirror A, and also locating the beam on the reference position on the roof. However, it serves as a starting point for a more accurate alignment.

I.2 Optical alignment method

Once the laser and telescope are aligned as in the approximate method, a more accurate alignment can then be achieved by the following procedure:

(i)   A large mirror is mounted on the roof in the centre of the aperture, at 45° to the vertical, to deflect the field of view and transmission back to the horizontal direction. This mirror, shown in figure AI-1, is constructed by attaching a 75 mm gold plated laser mirror to a 300 x 180 mm aluminium back plate via a laser mirror holder which can be adjusted relative to the back plate. An aluminium coated glass mirror with a 90 mm hole in its centre is then attached to the same back plate using small blobs of silastic between the two surfaces, to allow for differential thermal expansion.   The plane of the central laser mirror (hereafter called laser roof mirror) is then adjusted so that its plane is parallel to the roof mounted large rectangular glass mirror used for collecting light for the telescope. Although this glass

mirror deviates from a plane surface by several wavelengths across its surface at the CO_2 frequency, this will not affect the alignment procedure.

(ii)   Once the roof mirror system is set up, the laser beam is directed at a target van located 450 m away.   The laser beam is centered on the target van by using a small 75 mm loudspeaker to sense the laser pulse impact.   The light energy is converted to sound energy by thermal expansion of the surface on which the beam impacts.   The laser beam section is mapped out approximately by using the acoustic output pulse level of the speaker as a measure of beam intensity.   At the target van the beam shape will be found to be elongated in the horizontal direction with two hot spots horizontally displaced.   This is in accord with the predicted diffraction-limited beam section which has a width 1.7 times the height.   The telescope is then visually centered on the target van reference, using a perspex disc with a crosshair located at the detector position (axially adjusted to allow for wavelength difference).

(iii) After the initial alignment (done at visible wavelengths with the telescope) a 1 x 1 mm pyroelectric detector (Molection Pl-61) is placed at the CO_2 laser far field focussing position.   This is done to avoid the possibility of damage to the mercury-cadmium-telluride (CMT) detector by exposure to high power infra-red reflections during the alignment, and the necessity of cooling the detector to $77^\circ K$, which involves filling the dewar flask with liquid nitrogen.   Calculations indicate that, using a pyroelectric detector which has a detectivity of 5×10^9 cm√Hz/W and bandwidth of approximately 100 Hz, an echo should be received.   Following the initial laser alignment, an echo could not be detected at first with this procedure,   so a metal corner reflector was constructed with side length 750 mm to facilitate alignment.   This was placed in the centre of the target van and strong echos were received. Later, when the alignment procedure was repeated, it was demonstrated that discernible echos could be received directly from the side of the target van (a matt white painted metal surface), in agreement with the initial prediction.
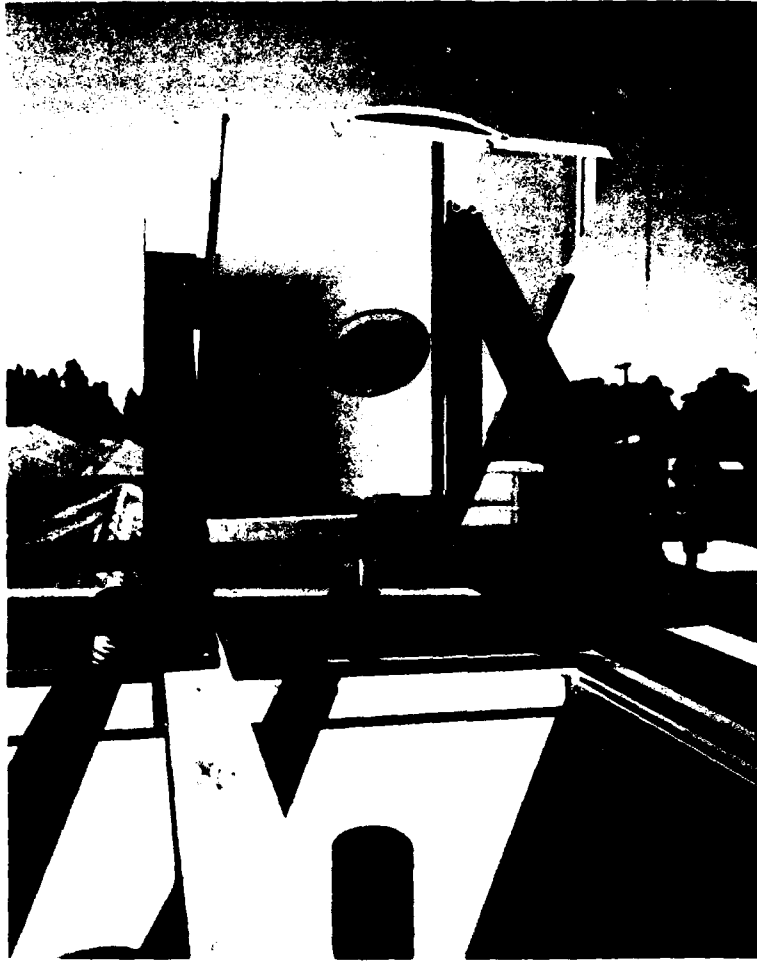
Figure I.1   Roof mirror assembly.   Gold-coated laser mirror is mounted at
             centre

APPENDIX II

ELECTRONIC CONTROL, SIGNAL PROCESSING AND DATA LOGGING SYSTEMS (REFER TO FIGURE II-1)

II.1 Laser control unit

(a) Provides electrical power supplies, trigger pulse and PRF control to CO_2 laser.

(b) Mixes CO_2, Helium and Nitrogen gases, and regulates flow to laser. Also supplies nitrogen gas to laser HV trigger spark gap.

II.2 CO_2 Laser

Consists of:

(a) High voltage trigger power supply and spark gap.

(b) Three section CO_2 laser with energy storage capacitors.

(c) Front and rear optics with micrometer adjustable wavelength grating at rear.

II.3 Automatic laser tuning system

Automatically drives laser tuning grating alternately between any two selected wavelengths after each transmitted pulse. The system consists of:

(a) A programmable counter unit with internal clock source. After each transmit pulse this unit provides a pre-selected number of output pulses and a direction reversal signal for stepping motor control.

(b) A stepping motor drive unit which provides power supplies and logic for stepping motor drive.

(c) Stepping motor and gear assembly which is mechanically coupled to laser tuning micrometer.

II.4 Remote tuning position indicator

Consists of:

(a) A photo-coupler and amplifier mounted adjacent to the laser wavelength tuning micrometer drive gear.

(b) A remote LED indicator which is illuminated when a reflective strip on the tuning drive gear aligns with the photo-coupler. This corresponds to the reference wavelengths.

II.5 Monitor detector

Samples/detects laser output pulse and provides an amplitude reference level for each transmitted pulse.

II.6 Signal detector

(a) Receives/detects signal backscatter from atmosphere via telescope.

(b) The logarithmic amplifier is employed to effectively increase dynamic range by compressing signal amplitude to match input range of A to D converter.

11.7 Signal gate, switch and sum

Performs gating of monitor (transmission sample) and received backscatter signals and provides a sequential (time multiplexed) output of same via a summing and amplifier.

11.8 Fast A to D converter and random access memory

(a) A 6 bit parallel A to D converter converts combined monitor and received signals to a digital format.

(b) The converted signal is stored in random access memory.

(c) The 6 MHz clock generator determines sampling rate and range resolution of 25 m.

11.9 Microprocessor system

(a) The microprocessor system is based on an "Intel" 8080 CPU.

(b) The microprocessor is used to control and interface the operation of peripheral units and to process and output the collected data.

(c) A video display unit and keyboard allow some interaction between the operator and the data collection system.

(d) The programme is contained in erasable read only memory, providing ease of modification and change.

11.10 Data recording

Collected data comprises 260 samples per pulse (signal followed by monitor) and time of day, and is recorded as follows:

(a) On punch paper tape (ASC11 code)

(b) On printer (hexadecimal)

(c) On storage oscilloscope and photographic film (analog).

NOTE: Reference 8 provides a complete technical description
      of the sounder and data logging systems with relevant
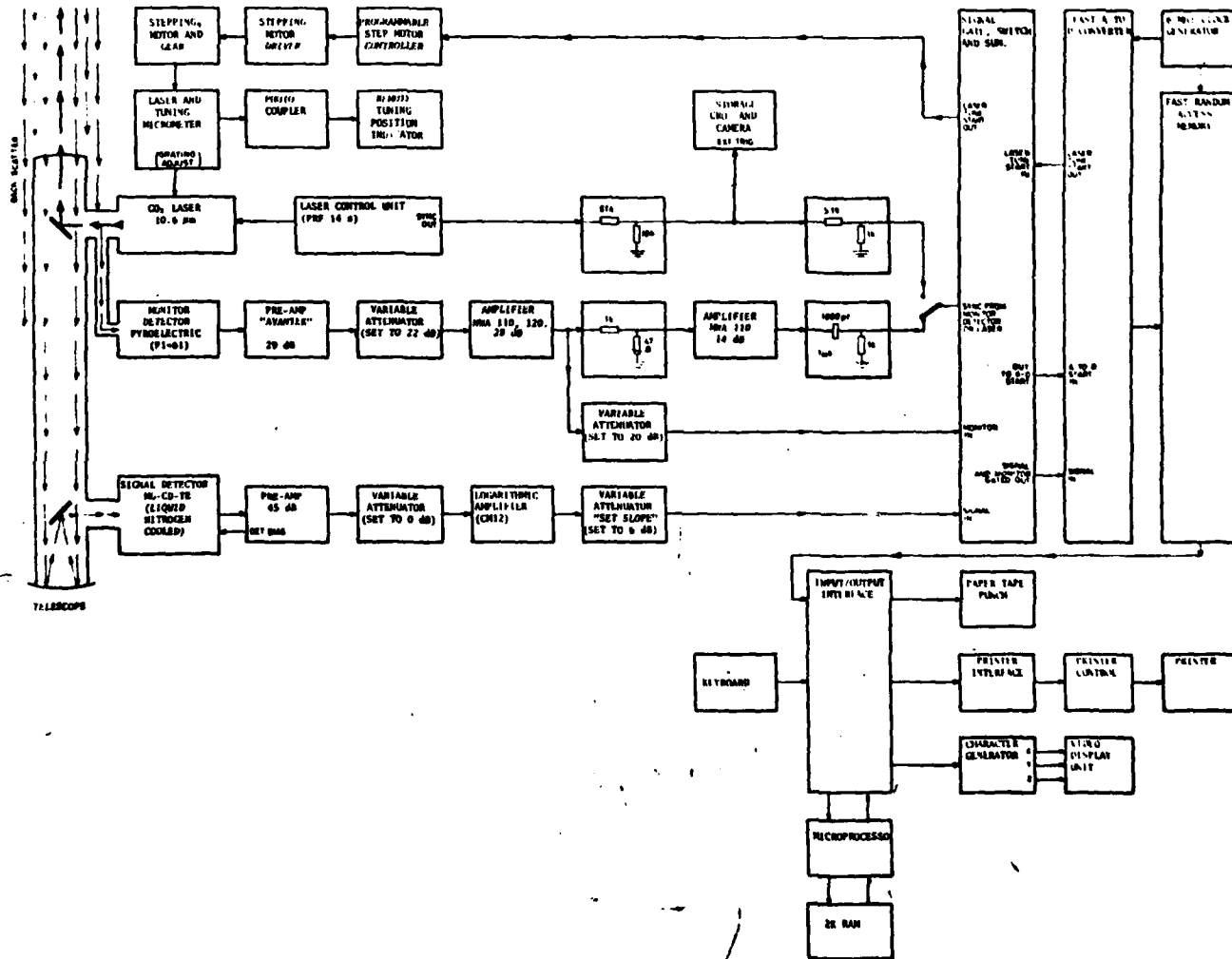   drawings and circuit diagrams included.

Figure II.1 Electronic control, signal processing and data logging systems

APPENDIX III

PULSE TAIL EFFECTS

If the pulse is considered to comprise a sharp leading edge followed by an exponential decay of the form $\exp(-t/TAU)$, where t is the time delay after the leading edge and TAU is the pulse length, then when the leading edge is returned from a range R, a point on the trailing edge of the pulse at x, corresponding to a time interval $\frac{2(R-x)}{C}$, will arrive back at the receiver at the same time as the leading edge. The total energy received at a given instant from all backscattered components of the pulse is proportional to

$$\int_{x=0}^{R} \exp\left\{-\frac{2(R-x)}{TAU \times C}\right\} \exp\left\{-\frac{x}{HS}\right\} \exp\left\{-\frac{2\alpha xW}{0.622}\right\} / x^2 \, dx$$

where HS is the scale height of the aerosol density, W is the water vapour concentration (mixing ratio) profile and α is the absorption coefficient of water vapour on the absorbed wavelength emission. Combining this expression with one for the unabsorbed transmission yields the differential absorption ratio

$$\frac{\int_{x=0}^{R} \exp\left\{-\frac{2(R-x)}{TAU \times C}\right\} \exp\left\{-\frac{x}{HS}\right\} \exp\left\{-\frac{2\alpha xW}{0.622}\right\} / x^2 \, dx}{\int_{x=0}^{R} \exp\left\{-\frac{2(R-x)}{TAU \times C}\right\} \exp\left\{-\frac{x}{HS}\right\} / x^2 \, dx}$$

This expression has been evaluated numerically for several values of TAU and HS. The water vapour mixing ration, W, was assumed to be 6 g/kg up to a height of 1 km and zero at greater heights. The curves in figure III.1 show the reduction in the returned power differential (in decibels) at short ranges as the pulse length is increased. Pulse lengths of 30 m and 300 m are representative of the CO_2 laser's short and long pulses respectively.

Figure III.1 illustrates that as the pulse length is increased the height at which the full differential absorption (due to the water vapour layer) is reached, suffers progressive delay.
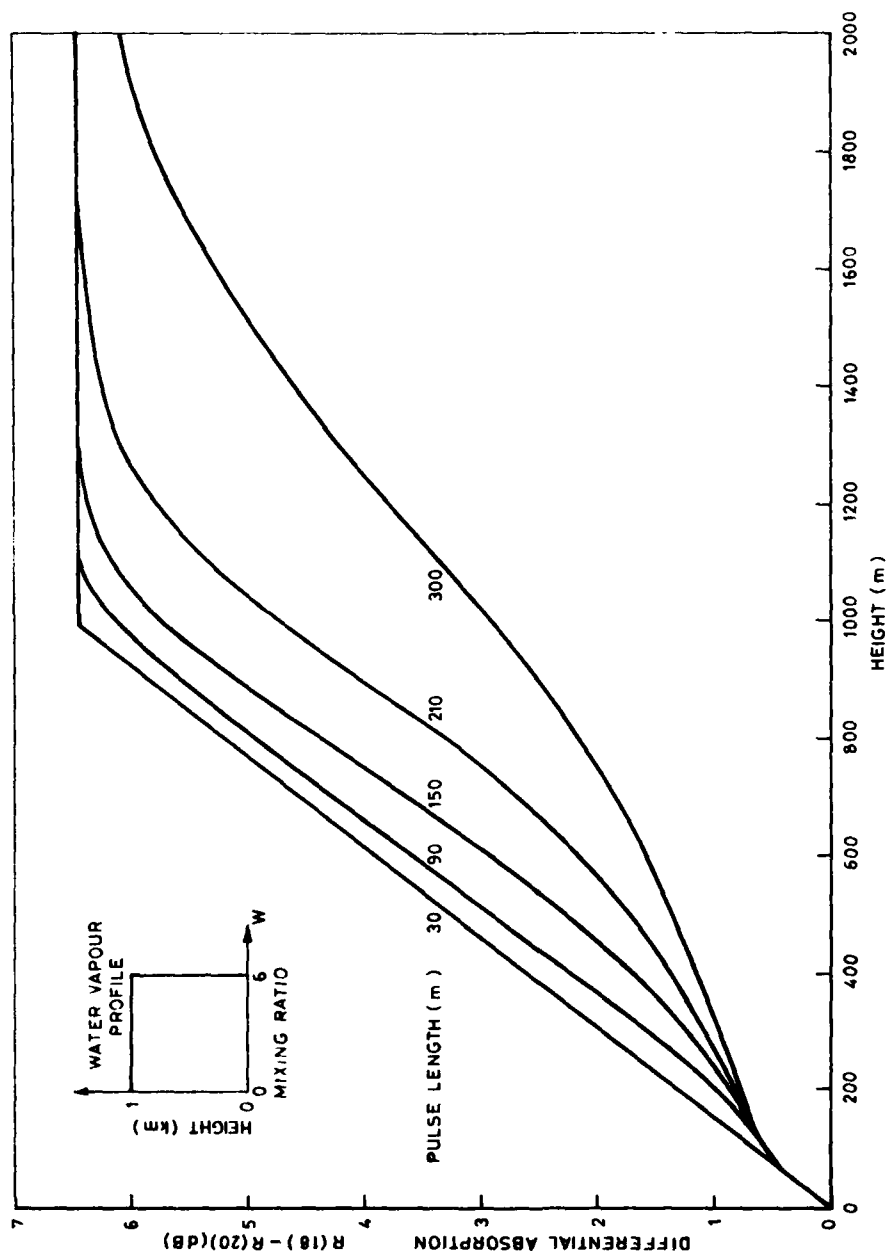
Figure III.1 Predicted differential absorption versus range for pulse lengths
representative of CO_2 laser output

APPENDIX IV

COMPUTATION OF RMS ERRORS IN WATER VAPOUR

The expression for the average mixing ratio (in grams/kilogram) between the ith and (i+1)th range cells may be written

$$W(i) = \frac{622}{2\Delta K \Delta R} \ln\left[\frac{P_1(i+1)P_2(i)}{P_1(i)P_2(i+1)}\right]$$

where $\Delta R = R_{i+1} - R$; $P_1(i)$ is the average power received (over N pulses) for a transmission wavelength λ_1 and λ_2 $(km^{-1}atm^{-1})$.

The error for $W(i)$ may be written

$$\Delta W(i) = \frac{\partial W}{\partial P_1(i)} \Delta P_1(i) + \frac{\partial W}{\partial P_1(i+1)} \Delta P_1(i+1) \ldots\ldots$$

$$= \frac{622}{2\Delta K \Delta R}\left\{\frac{\Delta P_2(i)}{P_2(i)} + \frac{\Delta P_1(i+1)}{P_1(i+1)} - \frac{\Delta P_2(i+1)}{P_2(i+1)} - \frac{\Delta P_1(i)}{P_1(i)}\right\}$$

Therefore the rms error in W is given by

$$\Delta W_{rms} = \frac{622}{2\Delta R \Delta K}\left\{\frac{\Delta P_1^2(i)}{P_1^2(i)} + \frac{\Delta P_2^2(i+1)}{P_2^2(i+1)} + \frac{\Delta P_1^2(i+1)}{P_1^2(i+1)} + \frac{\Delta P_2^2(i)}{P_2^2(i)}\right\}^{\frac{1}{2}}$$

For computational purposes the mean square error over 2n+1 range cell estimates can be written

$$(\Delta W_j)^2 = \frac{622^2}{4\Delta R^2 \Delta K^2(2n+1)}\left\{\frac{\Sigma\sigma_{18}^2(i)}{(\Sigma P_{18}(i))^2} + \frac{\Sigma\sigma_{20}^2(i)}{(\Sigma P_{20}(i))^2} + \frac{\Sigma\sigma_{18}^2(i+1)}{(\Sigma P_{18}(i+1))^2} + \frac{\Sigma\sigma_{20}^2(i+1)}{(\Sigma P_{20}(i+1))^2}\right\}$$

where σ^2 is the variance, with the mean removed, of the average power estimates in the 25 m range cells, and Σ is as defined for equations (1), (2), (3) and (4).

APPENDIX V

THE EFFECT OF AN ELEVATED AEROSOL LAYER ON THE MEASUREMENT OF A DIFFERENTIAL
ABSORPTION PROFILE

The differential absorption model introduced in Appendix III has been employed
to predict the effects of an elevated aerosol layer on differential absorption
measurements.   The curve in figure V.1 was obtained using the following
parameters:

   Normalized aerosol backscatter function, $\beta = \exp(-h/HS)$

   Layer backscatter function, $\beta = 30 \exp(\frac{-700}{HS})$

   Layer position $= 700$ to 1000 m

   Background scale height, $HS = 200$ m

   Water vapour mixing ratio profile $W = 6$ g/kg $0 < h < 1000$ m
                                              $= 0$ $h > 1000$ m.

The aerosol backscatter function is also shown in figure V.1.   In addition to
the above parameters the inverse range squared dependence of the integrands of
the integrals in Appendix III were assumed to commence at a range of 50 m.   In
the range interval 0 to 50 m the inverse range squared function was replaced
by a linearly increasing function.   This allows for masking effects of the
telescope in this region and also closely predicts the actual returned power
distribution as a function of range.

The differential absorption profile which was obtained has three main
features.   The initial slowly changing section is mainly determined by the
combination of the pulse length and scale height parameters and hence the
gradient of this section can accordingly be varied by changing these
parameters.   Reducing HS reduces the differential absorption at all levels.
Secondly, the increasing section commencing at 700 m is due to the influence
of the aerosol layer which gives rise to an enhanced contribution from the
leading edge of the pulse.   Finally, the flattening of the curve occurs when
the leading edge of the pulse emerges from the top of the layer and the return
from the tail of the pulse is enhanced.

The dashed curve in figure V.1 is for a short pulse sounding and indicates the
error contained in the long pulse result.   There is only a slight kink in this
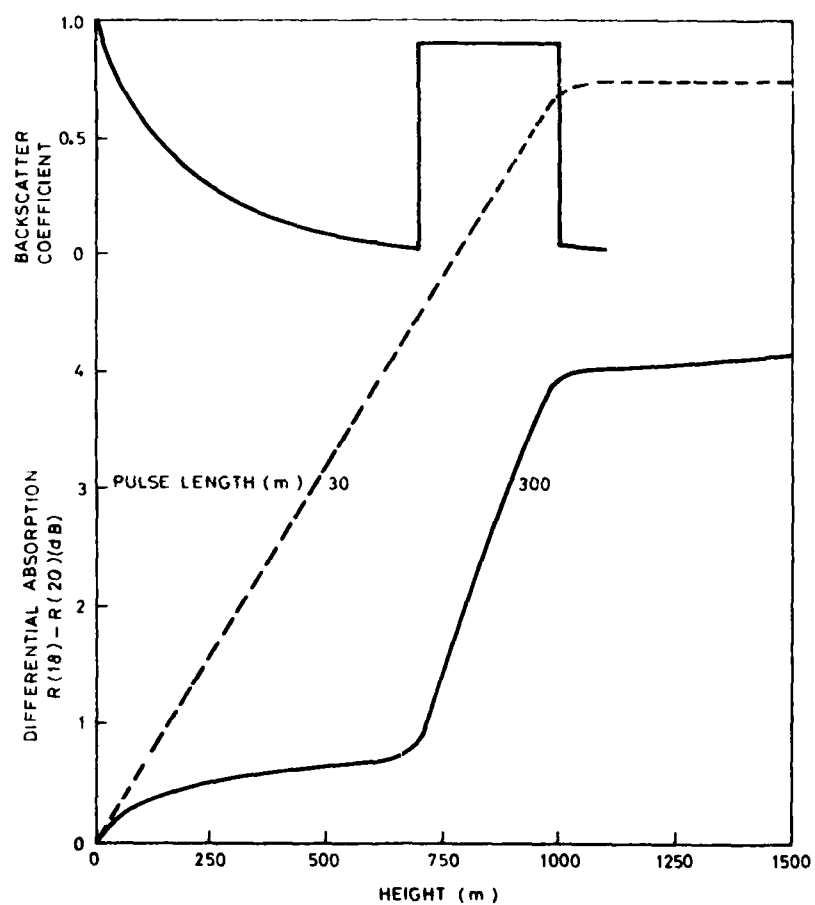curve at 700 m, at the base of the elevated aerosol layer.

Figure V.1 Predicted differential absorption versus range for assumed aerosol
density distribution

DISTRIBUTION

Copy No.

EXTERNAL

In United Kingdom

   Defence Science Representative, London   No copy

   British Library, Lending Division
    Boston Spa York   1

   Institution of Electrical Engineers
    Hitchin Herts SG5 IRJ   2

In United States of America

   National Technical Information Service
    Springfield VA 22151   3

   Counsellor, Defence Science, Washington   No copy

In Australia

   Chief Defence Scientist   4

   Deputy Chief Defence Scientist   5

   Superintendent, Science and Technology Programmes   6

   Director, Joint Intelligence Organization (DSTI)   7

   Superintendent, RANRL   8

   Navy Scientific Adviser   9

   RAAF Academy, University of Melbourne
    (Attention: Professor J.A. Thomas)   10

   Footscray Institute of Technology
    (Attention: Mr D. Booth)   11

   Atmospheric Physics Division, CSIRO, Melbourne
    (Attention: Dr B. Tucker)   12

   Library, W.A. Institute of Technology   13

   Library, Telecom Australia Research Laboratories,
    Clayton, Victoria   14

   Document Exchange Centre
    Defence Information Services Branch (for microfilming)   15

   Defence Library, Campbell Park   16

   Library, Aeronautical Research Laboratories   17

   Library, Materials Research Laboratories   18

DOCUMENT CONTROL DATA SHEET

Security classification of this page | UNCLASSIFIED |

1	DOCUMENT NUMBERS		2	SECURITY CLASSIFICATION
AR Number: AR-002-824			a. Complete Document: Unclassified	
Series Number: ERL-0230-TM			b. Title in Isolation Unclassified	
Other Numbers:			c. Summary in Isolation: Unclassified	

3	TITLE
	ATMOSPHERIC WATER VAPOUR DIFFERENTIAL ABSORPTION MEASUREMENTS WITH AN INFRARED SOUNDER

4	PERSONAL AUTHOR(S):
	P.W. Baker

5	DOCUMENT DATE:
	March 1982

6	6.1 TOTAL NUMBER OF PAGES 52
	6.2 NUMBER OF REFERENCES: 8

7	7.1 CORPORATE AUTHOR(S):
	Electronics Research Laboratory
	7.2 DOCUMENT SERIES AND NUMBER Electronics Research Laboratory 0230-TM

8	REFERENCE NUMBERS
	a. Task: DST 77/016
	b. Sponsoring Agency:

9	COST CODE:
	130924

10	IMPRINT (Publishing organisation)
	Defence Research Centre Salisbury

11	COMPUTER PROGRAM(S) (Title(s) and language(s))

12	RELEASE LIMITATIONS (of the document):
	Approved for Public Release

Security classification of this page: | UNCLASSIFIED |

Security classification of this page: | UNCLASSIFIED |

| 13 | ANNOUNCEMENT LIMITATIONS (of the information on these pages): |

No limitation

| 14 | DESCRIPTORS: | Water vapour   Air water inter- | 15 | COSATI CODES: |

a. EJC Thesaurus Terms

Water vapour   Air water inter-
Moisture content   actions
Carbon dioxide lasers   Sounding
Remote systems
Refractivity sounding
Atmospheric composition

2014

b. Non-Thesaurus Terms

Lidar

| 16 | SUMMARY OR ABSTRACT:
(if this is security classified, the announcement of this report will be similarly classified)

The atmospheric differential absorption by water vapour between two CO_2 laser transmission lines has been measured up to heights of 1.5 km with a groundbased sounder system. Water vapour profiles, some containing distinct layers, have been estimated from long and short pulse soundings, and compared with radiosonde measurements. Strongly scattering aerosol layers, often associated with temperature inversions, cause severe distortion of the long pulse differential absorption profiles, indicating the necessity of using a short pulse technique. This technique shows potential usefulness for the remote measurement of radio refractive index layers in the atmosphere.

END

DATE
FILMED

1-83

DTIC